# Novel azo pyridone dyes based on dihydropyrimidinone skeleton: Synthesis, DFT study and anticancer activity

Julijana D. Tadić[a], Jelena M. Lađarević[b,*], Željko J. Vitnik[c], Vesna D. Vitnik[c], Tatjana P. Stanojković[d], Ivana Z. Matić[d], Dušan Ž. Mijin[b]

[a]Innovation Centre of Faculty of Technology and Metallurgy in Belgrade, Karnegijeva 4, Belgrade, Republic of Serbia

[b]Faculty of Technology and Metallurgy, University of Belgrade, Karnegijeva 4, Belgrade, Republic of Serbia

[c]Department of Chemistry, Institute of Chemistry, Technology and Metallurgy, University of Belgrade, Studentski trg 12-16, Belgrade, Republic of Serbia

[d]Institute of Oncology and Radiology of Serbia, Pasterova 14, Belgrade, Republic of Serbia

*Corresponding author.

E-mail: jmirkovic@tmf.bg.ac.rs

## Abstract

Seven novel azo dyes with 2-pyridone and dihydropyrimidinone moieties have been synthesized and thoroughly characterized. The azo-hydrazone tautomerism has been investigated by experimental and theoretical approaches. The optimizations of geometries have been performed with density functional theory (DFT). The vibrational and NMR spectra were calculated and correlated with experimental ones. Furthermore, quantum chemical descriptors were calculated and MEP maps were plotted to determine biological reactivity of dyes. The antioxidant assay evinced that **5**, **6** and **7** are promising antioxidant candidates. *In vitro* cytotoxic activity was studied against three malignant cell lines: prostate adenocarcinoma (PC-3), lung carcinoma (A549) and

chronic myelogenous leukemia (K562), as well as against human normal lung fibroblasts (MRC-5), using MTT assay. Examination of cytotoxic effects on human cancer cell lines showed the concentration dependent cytotoxicity of all investigated compounds. The K562 cells were the most sensitive to the cytotoxicity of the compounds **3**, **5** and **6**, wherein compound **5** was particularly prominent and selective in cytotoxic action between K562 (24.97 μM) and PC-3 (48.98 μM) cancer cells, and normal MRC-5 (91.11 μM) cells. Moreover, the cell cycle analysis of compound **5** was examined in K562 cells, by flow cytometry, to study its mechanism of anticancer action. Finally, *in silico* evaluation of physicochemical parameters, druglikeness and ADME properties showed that investigated compounds are orally bioavailable with no permeation to the blood brain barrier.

Keywords: Biginelli adduct, azo-hydrazone tautomerism, antitumor, cell cycle arrest, ADME

## 1. Introduction

Azo dyes are the most significant class of colored synthetic compounds. They have diverse application in various fields of science and industry, regarding their simple preparation and a broad spectrum of derivatives [1]. The synthesis of azo dyes based on heterocycle moieties has gained particular attention in last several decades [2,3]. Namely, the heterocyclic azo compounds exhibit antibacterial [4], antifungal [5], antioxidant [6], analgesic [7], anti-inflammatory [8], antitubercular [9] and anticancer properties [10, 11]. Moreover, studies on new antitumor drugs have reviled that some azo compounds manifest cytotoxic action against EAC (Ehrlich-Lettre ascites carcinoma), MCF-7 and MDA-MB-231 (breast cancer), PC-3 (human prostate cancer) and K562 (myelogenous leukemia) tumor cells [12].

Among this class of azo dyes, those with 2-pyridone moiety in the structure are particularly significant. Besides their remarkable coloration properties [13], azo pyridone dyes exhibit

antibacterial activity [14] and demonstrate the potency for cancer therapy [15]. One of the most investigated feature of azo pyridone dyes is the phenomenon of azo-hydrazone tautomerism [16-18]. The structural characterization of the dyes is crucial, since the tautomeric forms differ in physical properties and thus, biological activity [19].

On the other side, dihydropyrimidinone scaffold (DHPM or dihydropyrimidine-5-carboxylate core) is a heterocyclic system which has been synthesized *via* Biginelli reaction, including one-pot multicomponent reaction of an aromatic aldehyde, urea and ethyl acetoacetate [20]. The Biginelli synthesis is exceptionally attractive allowing development of numerous DHPM derivatives by simple variation of the starting components [21]. Furthermore, the compounds based on the dihydropyrimidine-5-carboxylate core have shown remarkable biological properties such as antibacterial, antiviral, antiinflammatory, antioxidant and antitumor activity [22]. Recently, DHPM based compounds have emerged as the calcium channel blockers, potential therapeutics against Alzheimer's disease, potential new AIDS therapy, the antihypertensive agents and potent breast cancer therapy [23].

In this manner, we merged dihydropyrimidinone based core with seven different 2-pyridones *via* reaction of diazo coupling, designing a novel series of azo pyridone dyes. Since 2-pyridone and DHPM moieties manifest biological activity, their conjugation can ameliorate biological properties of azo dyes. Contrary to the traditional arylazo dyes, where aniline-based compounds are the most commonly employed as diazotization agenesis, hereby, we use the Biginelli adduct. The substitution of aryl diazonium salts with DHPM-diazo moiety, leads to elimination of highly toxic degradation products of azo dyes, since Biginelli adducts exhibit negligible toxicity [24]. Besides, there are only few studies of DHPM-azo dyes [25,26], and according to our best knowledge, DHPM-azo pyridone dyes have been unexplored. Nevertheless, cancer is one of the

main targets in therapeutic chemistry, so we made an effort to design azo molecules with potential anticancer activity.

Herein, the synthesis, structural characterization and azo-hydrazone tautomerism of seven novel DHPM-azo pyridone dyes have been reported. The structures of molecules have been confirmed by ATR-FTIR, NMR, UV-Vis, MS and elemental analysis. The calculated structural and spectroscopic properties of dyes have been investigated with density functional theory (DFT). The calculated vibrational spectrum of the hydrazone tautomer has been correlated with the experimental one. The nuclear magnetic resonance (NMR) chemical shifts of the hydrazone tautomer have been calculated and compared with experimental data. Molecular Electrostatic Potential (MEP) surfaces are plotted over the optimized geometry to brighten the reactivity of investigated molecules. Furthermore, the biological reactivity of novel azo molecules has been correlated with 14 quantum chemical descriptors. The antioxidant activity has been evaluated by ABTS (2,2'-azinobis-(3-ethylbenzothiazoline-6-sulfonic acid)) assay. *In vitro* antitumor action of dihydropyrimidinone (**B2**, Figure 1) and DHPM-azo dyes (**1-7,** Figure 1) was determined against following tumor cell lines: prostate adenocarcinoma (PC-3), lung carcinoma (A549), chronic myelogenous leukemia (K562), and human normal lung fibroblast (MRC-5) using microculture tetrazolium test (MTT) assay. Additionally, cell cycle analysis of the most active compound (**5,** Figure 1) was examined in K562 cells in order to enlighten the antitumor properties. The effect of dye **5** on the cell cycle was measured by flow cytometry. Finally, physicochemical parameters, druglikeness and ADME properties of novel compounds were evaluated *in silico* by SwissADME and Vega 22.

## 2. Experimental part

### *2.1. Materials and Measurements*

All starting materials were purchased from Merck, Fluka and Acros, and were used without further purification. The microwave-assisted organic synthesis was performed on Anton Paar Monowave 300. The chemical structures of the synthesized compounds were confirmed by melting points, elemental analysis, ATR-FTIR, $^{1}$H-NMR, $^{13}$C NMR, ESI-MS and UV-Vis spectral data. The melting points were determined in capillary tubes on an automated melting point system Stuart SMP30. Elemental analysis was done on Vario EL III elemental analyzer. Fourier transform infrared spectroscopy (FT-IR) spectra of the dyes were recorded in absorbance mode, using a Nicolet™ iS™ 10 FT-IR Spectrometer (Thermo Fisher Scientific) with Smart iTR™ Attenuated Total Reflectance (ATR) sampling accessories. The ATR-FTIR spectra were recorded in the 500–4000 $cm^{-1}$ range with 20 scans per spectrum. The $^{1}$H-NMR and $^{13}$C NMR spectral measurements were performed on a Bruker Ascend 400 instrument (400 Hz and 100 MHz, respectively) in deuterated dimethylsulfoxide (DMSO-$d_6$) and deuterated trifluoroacetic acid for **7** ($CF_3COOD$). The chemical shifts were expressed in ppm values referenced to tetramethylsilane (TMS). Quadrupole ion trap mass spectrometer (LCQ Advantage (Thermo Fisher Scientific, USA) was used for the compounds detection. The electrospray ionization technique (ESI) was used and compounds were analyzed in the positive and negative ionization mode. The optimal source working parameters for monitoring ions in positive and negative mode were: source voltage – 4.5 kV, sheath gas – 28 au, *i.e*. 28 arbitrary units, auxiliary gas – 4 au, capillary temperature – 220 °C and capillary voltage 3 V for ESI+, or – 26 V for ESI–. The ultraviolet-visible (UV-Vis) absorption spectra were recorded in ethanol, on a Schimadzu 1700 spectrophotometer, at concentration $4 \times 10^{-5}$ mol $L^{-1}$. All spectroscopic measurements were carried out at room temperature (25 °C).

*2.2. Synthesis*

To the best of our knowledge, synthesis of azo pyridone dyes with dihydropyrimidinone moiety, has not been reported in literature. In this study seven novel DHPM-azo dyes were obtained by following synthetic pathway given in Figure 1. In the first step, synthesis of ethyl 6-methyl-4-(4-nitrophenyl)-2-oxo-1,2,3,4-tetrahydropyrimidine-5-carboxylate (**B1**) was performed according to modified literature procedure, wherein the reaction time was elongated in regard to the reported method [21]. Second step includes the reduction of **B1** in order to produce Biginelli adduct 4-(4-aminophenyl)-6-methyl-2-oxo-1,2,3,4-tetrahydropyrimidine-5-carboxylate (**B2**) [27]. In the third step, seven different 6-hydroxy-2-pyridones (**P1-7**) were obtained using literature methods [28, 29] (the synthetic details are given in Supplementary material). Finally, seven novel azo dyes **1-7** were synthesized *via* diazotization reaction of dihydropyrimidinone (**B2**) followed by coupling reaction, of the resulting diazonium salt (**B3**), with corresponding pyridones (**P1-7**).

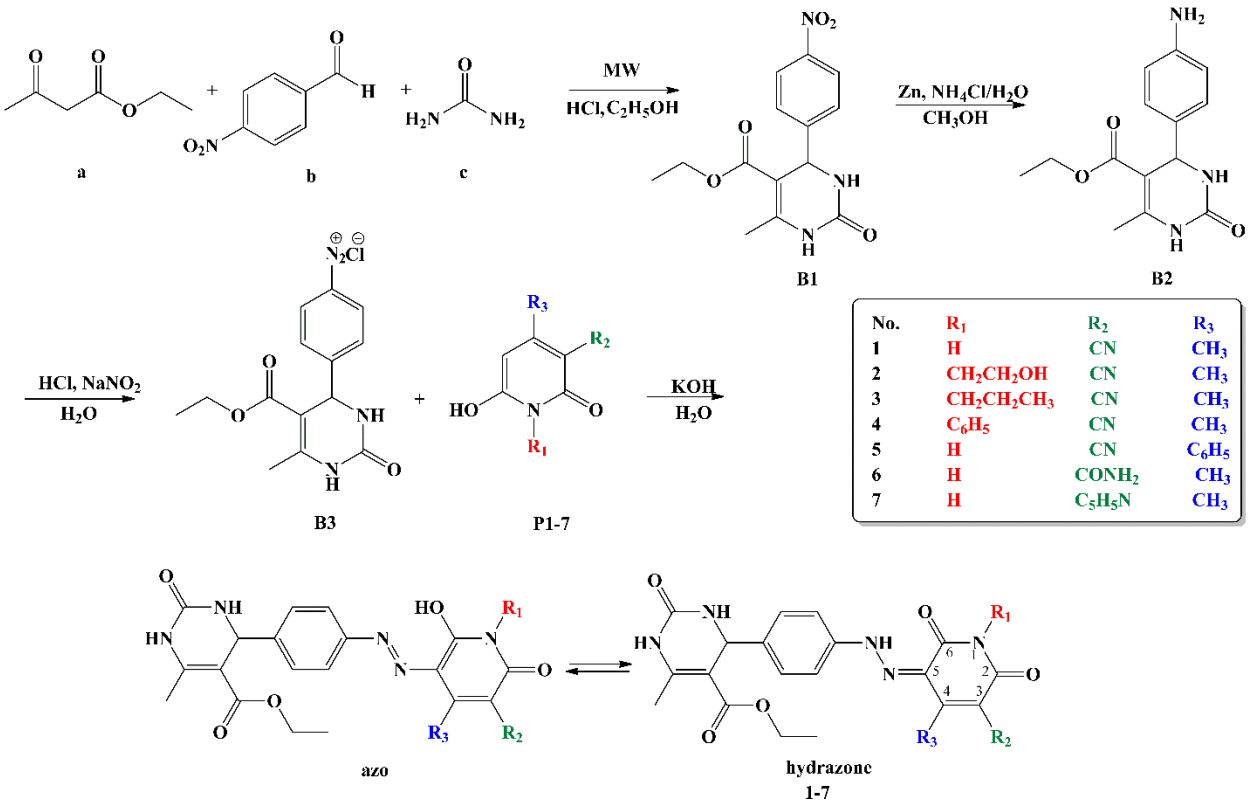


Figure 1. The synthetic pathway of novel DHPM-azo pyridone dyes.

*2.2.1. Synthesis of ethyl 6-methyl-4-(4-nitrophenyl)-2-oxo-1,2,3,4-tetrahydropyrimidine-5-carboxylate (**B1**)*

Ethyl acetoacetate (**a**) (4 mmol, 0.510 ml), 4-nitrobenzaldehyde (**b**) (4 mmol, 0.604 g) and urea (**c**) (4 mmol, 0.240 g) were dissolved in 10 ml of ethanol, and 4 drops of hydrochloric acid were added (Figure 1). The reaction mixture was heated in the microwave reactor at 120 °C for 30 minutes. When the reaction was completed, the obtained mixture was left at 4 °C for 24 hours. The crude product was filtered on a Buchner funnel, washed with ethanol, air dried and then recrystallized from ethanol. The structure of **B1** was confirmed by ATR-FTIR and NMR analysis, and has been in accordance with literature data [21]: white crystals; yield 68 %; m.p. 204–205 °C; ATR-FTIR ($\nu$/cm$^{-1}$): 3225 (NH), 3111 (NH), 1720 (CO), 1636 (CO); $^{1}$H NMR (400 MHz, DMSO-$d_6$, $\delta$/ppm): 1.10 (3H, t, $J$ = 7.2 Hz, $COOCH_2C\underline{H}_3$), 2.27 (3H, s, $CH_3$), 3.99 (2H, q, $J$ = 7.2 Hz, $COOC\underline{H}_2CH_3$), 5.27 (1H, d, $J$ = 2.8 Hz, C–H), 7.51 (2H, d, $J$ = 8.8 Hz, Ar–H), 7.91 (1H, s, NH), 8.23 (2H, d, $J$ = 8.4 Hz, Ar–H), 9.38 (1H, s, NH); $^{13}$C NMR (200 MHz, DMSO-$d_6$, $\delta$/ppm): 14.53 ($COOCH_2\underline{C}H_3$), 18.35 ($CH_3$), 54.13 (C–H), 59.87 ($COO\underline{C}H_2CH_3$), 98.62 ($\underline{C}$–$COOCH_2CH_3$, DHPM), 124.33 (Ar), 128.13 (Ar), 147.18 (Ar), 149.88 (Ar), 152.21 ($\underline{C}$–$CH_3$, DHPM), 152.46 (CO, DHPM), 165.22 ($\underline{C}OOCH_2CH_3$).

*2.2.2. Synthesis of ethyl 4-(4-aminophenyl)-6-methyl-2-oxo-1,2,3,4-tetrahydropyrimidine-5-carboxylate (**B2**)*

**B1** (2 mmol, 0.670 g) was dissolved in 40 ml of methanol and its reduction was carried out by the addition of zinc (20 mmol, 1.438 g) and aqueous solution of ammonium chloride (4 mmol, 0.235 g in 4 ml of water). The reaction was followed by TLC, and conducted at reflux for 5 hours. The reaction mixture was filtered and the filtrate was left at 4 °C for 24 hours. The resulting **B2** was separated on a Buchner funnel, washed with ethanol, air dried and recrystallized from ethanol:

white crystals; yield 62 %; m.p. 212–213 °C; ATR-FTIR ($\nu$/cm$^{-1}$): 3531, 3383 ($NH_2$), 3211 (NH), 3104 (NH), 1681 (CO), 1635 (CO); $^1$H NMR (400 MHz, DMSO-$d_6$, $\delta$/ppm): 1.11 (3H, t, $J$ = 7.2 Hz, $COOCH_2C\underline{H_3}$), 2.22 (3H, s, $CH_3$), 3.98 (2H, q, $J$ = 7.2 Hz, $COO\underline{CH_2}CH_3$), 4.97 (1H, s, C–H), 4.98 (2H, s, $NH_2$), 6.47 (2H, d, $J$ = 8 Hz, Ar–H), 6.88 (2H, d, $J$ = 8 Hz, Ar–H), 7.52 (1H, s, NH), 9.03 (1H, s, NH); $^{13}$C NMR (200 MHz, DMSO-$d_6$, $\delta$/ppm): 14.59 ($COOCH_2\underline{C}H_3$), 18.17 ($CH_3$), 54.02 (C–H), 59.49 ($COO\underline{C}H_2CH_3$), 100.48 ($\underline{C}$–$COOCH_2CH_3$, DHPM), 114.01 (Ar), 127.72 (Ar), 132.77 (Ar), 147.78 (Ar–$NH_2$), 148.30 ($\underline{C}$–$CH_3$, DHPM), 152.70 (CO, DHPM), 165.99 ($\underline{C}OOCH_2CH_3$); Anal. Calcd for $C_{14}H_{17}N_3O_3$ (275.30): C, 61.08; H, 6.22; N, 15.26%; Found: C, 61.18; H, 6.35; N, 15.37%; ESI-MS m/z calc. 275.13, found (positive mode): 276.08 $[M+H]^+$, 550.95 $[2M+H]^+$, 572.92 $[2M+Na]^+$.

*2.2.3. Synthesis of DHPM-azo pyridone dyes*

**B2** (1 mmol, 0.275 g) was dissolved in the diluted hydrochloric acid (3 ml of HCl (37% w/w) and 60 ml of water) and then cooled to 0–5 °C. Sodium nitrite (1.1 mmol, 0.0759 g) was dissolved in cold water (4 ml) and added dropwise to a solution of **B2**. The mixture was stirred in an ice bath for 1 hour in order to obtain diazonium chloride (**B3**). The corresponding 6-hydroxy-2-pyridone (**P1-7**) (1 mmol) was dissolved in an aqueous solution of potassium hydroxide (1 mmol, 0.056 g and 10 ml of water) and then cooled to 0–5 °C. The obtained diazonium chloride (**B3**) was added dropwise to the corresponding pyridone solution. The resulting reaction mixture was stirred for 3 hours and maintained at 0–5 °C. When the reaction was completed the obtained azo dyes (**1-7**) were filtered on a Buchner funnel, washed with water, air dried and recrystallized from ethanol. All obtained dyes are characterized by melting points, ATR-FTIR, UV-Vis, ESI-MS, $^1$H and $^{13}$C NMR spectra and elemental analysis. In addition, the NMR analysis of dye **7** was performed in

$CF_3COOD$, due to the low solubility in DMSO-$d_6$. The ATR-FTIR, ESI-MS $^1H$ and $^{13}C$ NMR spectra for all dyes are provided in Supplementary material (Figures S1-S35).

*Ethyl 4-(4-((5-cyano-2-hydroxy-4-methyl-6-oxo-1,6-dihydropyridin-3-yl)diazenyl)phenyl)-6-methyl-2-oxo-1,2,3,4-tetrahydropyrimidine-5-carboxylate* ***(1)***. Dark orange powder; yield 73%; m.p. 249-250 °C; ATR-FTIR ($\nu$/cm$^{-1}$): 3296 (NH), 3211 (NH), 2219 (CN), 1674 (CO), 1622 (CO), 1506 (NH); $^1H$ NMR (400 MHz, DMSO-$d_6$, $\delta$/ppm): 1.10 (3H, t, $J$ = 7 Hz, $COOCH_2C\underline{H_3}$), 2.26 (3H, s, $CH_3$ DHPM), 2.51 (3H, s, $CH_3$ Py), 3.99 (2H, q, $J$ = 7 Hz, $COOC\underline{H_2}CH_3$), 5.17 (1H, d, $J$ = 3.2 Hz, C–H), 7.33 (2H, d, $J$ = 8.2 Hz, Ar–H), 7.64 (2H, d, $J$ = 8.2 Hz, Ar–H), 7.79 (1H, s, NH), 9.25 (1H, s, NH), 12.02 (1H, s, NH Py), 14.58 (1H, s, NH hydrazone); $^{13}C$ NMR (200 MHz, DMSO-$d_6$, $\delta$/ppm): 14.58 ($COOCH_2\underline{C}H_3$), 16.92 ($CH_3$, Py), 18.27 ($CH_3$, DHPM), 54.04 (C–H, DHPM), 59.73 ($COO\underline{C}H_2CH_3$), 99.38 ($\underline{C}$–$COOCH_2CH_3$, DHPM), 101.09 (CN), 115.59 ($\underline{C}$–CN), 117. 95 (Ar), 124.04 (C=N, Py), 128.17 (Ar), 140.73 (Ar), 144.04 (Ar), 149.13 ($\underline{C}$–$CH_3$, DHPM), 152.45 (CO, DHPM), 160.95 (Py), 161.32 (CO, Py), 161.97 (CO, Py), 165.72 ($\underline{C}OOCH_2CH_3$); Anal. Calcd for $C_{21}H_{20}N_6O_5$ (436.42): C, 57.79; H, 4.62; N, 19.26%; Found: C, 57.99; H, 4.92; N, 19.36%; ESI-MS m/z calc. 436.15, found (negative mode): 435.22 $[M–H]^–$; UV-Vis (EtOH) ($\lambda_{max}$/nm (log $\varepsilon$/mol$^{-1}$dm$^3$cm$^{-1}$)): 439.0 (4.55).

*Ethyl 4-(4-((5-cyano-2-hydroxy-1-(2-hydroxyethyl)-4-methyl-6-oxo-1,6-dihydropyridin-3-yl)diazenyl)phenyl)-6-methyl-2-oxo-1,2,3,4-tetrahydropyrimidine-5-carboxylate* ***(2)***. Orange powder; yield 71%; m.p. 195–196 °C; ATR-FTIR ($\nu$ /cm$^{-1}$): 3243 (NH), 2218 (CN), 1678 (CO), 1626 (CO), 1500 (NH); $^1H$ NMR (400 MHz, DMSO-$d_6$, $\delta$/ppm): 1.11 (3H, t, $J$ = 6.8 Hz, $COOCH_2C\underline{H_3}$), 2.27 (3H, s, $CH_3$ DHPM), 2.54 (3H, s, $CH_3$ Py), 3.56 (2H, t, $J$ = 6 Hz, $C\underline{H_2}CH_2OH$), 3.94–4.03 (4H, m, $CH_2C\underline{H_2}OH$, $COOC\underline{H_2}CH_3$), 5.18 (1H, d, $J$ = 2.8 Hz, C–H), 7.35 (2H, d, $J$ = 8.8 Hz, Ar–H), 7.70 (2H, d, $J$ = 8.8 Hz, Ar–H), 7.77 (1H, d, $J$ = 2 Hz, NH), 9.24 (1H, s, NH), 14.60

(1H, s, NH hydrazone); $^{13}$C NMR (200 MHz, DMSO-$d_6$, $\delta$/ppm): 14.58 ($COOCH_2\underline{C}H_3$), 16.77 ($CH_3$, Py), 18.27 ($CH_3$, DHPM), 41.92 ($CH_2\underline{C}H_2OH$), 54.05 (C–H), 57.91 ($\underline{C}H_2CH_2OH$), 59.72 ($COO\underline{C}H_2CH_3$), 99.42 ($\underline{C}$–$COOCH_2CH_3$), 100.88 (CN), 115.60 ($\underline{C}$–CN), 118.16 (Ar), 123.51 (C=N, Py), 128.16 (Ar), 140.77 (Ar), 144.18 (Ar), 149.13 ($\underline{C}$–$CH_3$, DHPM), 152.46 (CO, DHPM), 159.60 (Py), 160.66 (CO, Py), 161.18 (CO, Py), 165.73 ($\underline{C}OOCH_2CH_3$); Anal. Calcd for $C_{23}H_{24}N_6O_6$ (480.47): C, 57.49; H, 5.03; N, 17.49%; Found: C, 57.79; H, 5.15; N, 17.69%; ESI-MS m/z calc. 480.18, found (positive mode): 503.12 $[M+Na]^+$, 982.81 $[2M+Na]^+$, found (negative mode): 479.26 $[M–H]^–$; UV-Vis (EtOH) ($\lambda_{max}$/nm (log $\varepsilon$/$mol^{-1}dm^3cm^{-1}$)): 440.0 (4.50).

*Ethyl 4-(4-((5-cyano-2-hydroxy-4-methyl-6-oxo-1-propyl-1,6-dihydropyridin-3-yl)diazenyl)phenyl)-6-methyl-2-oxo-1,2,3,4-tetrahydropyrimidine-5-carboxylate* ***(3)****.* Orange powder; yield 65%; m.p. 160–161 °C; ATR-FTIR ($\nu$/$cm^{-1}$): 3593 (NH), 3507 (NH), 3220 (NH), 2233 (CN), 1709 (CO), 1677 (CO), 1621 (CO), 1514 (NH); $^1$H NMR (400 MHz, DMSO-$d_6$, $\delta$/ppm): 0.89 (3H, t, $J$ = 7.6 Hz, $CH_2CH_2C\underline{H}_3$), 1.11 (3H, t, $J$ = 6.8 Hz, $COOCH_2C\underline{H}_3$), 1.58 (2H, m, $CH_2C\underline{H}_2CH_3$), 2.27 (3H, s, $CH_3$ DHPM), 2.54 (3H, s, $CH_3$ Py), 3.82 (2H, t, $J$ = 7.2 Hz, $C\underline{H}_2CH_2CH_3$), 4.00 (2H, q, $J$ = 7.2 Hz, $COOC\underline{H}_2CH_3$), 5.18 (1H, d, $J$ = 2.8 Hz, C-H), 7.34 (2 H, d, $J$ = 8.4 Hz, Ar-H), 7.70 (2H, d, $J$ = 8.4 Hz, Ar-H), 7.77 (1H, s, NH), 9.23 (1H, s, NH), 14.62 (1H, s, NH hydrazone); $^{13}$C NMR (200 MHz, DMSO-$d_6$, $\delta$/ppm): 11.71 ($CH_2CH_2\underline{C}H_3$), 14.58 ($COOCH_2C\underline{H}_3$), 16.79 ($CH_3$, Py), 18.27 ($CH_3$, DHPM), 20.96 ($CH_2\underline{C}H_2CH_3$), 41.3 ($\underline{C}H_2CH_2CH_3$), 54.06 (C-H), 59.72 ($COO\underline{C}H_2CH_3$), 99.41 ($\underline{C}$-$COOCH_2CH_3$), 100.78 (CN), 115.60 ($\underline{C}$-CN), 118.17 (Ar), 123.48 (C=N, Py), 128.16 (Ar), 140.78 (Ar), 144.20 (Ar), 149.14 ($\underline{C}$–$CH_3$, DHPM), 152.45 (CO, DHPM), 159.68 (Py), 160.57 (CO, Py), 161.04 (CO, Py), 165.73 ($\underline{C}OOCH_2CH_3$); Anal. Calcd for $C_{24}H_{26}N_6O_5$ (478.50): C, 60.24; H, 5.48; N, 17.56%; Found: C, 60.49; H, 5.63; N,

17.78%; ESI-MS m/z calc. 478.20, found (negative mode): 477.18 $[M–H]^-$. UV-Vis (EtOH) ($\lambda_{max}$/nm (log ε/$mol^{-1}dm^3cm^{-1}$)): 442.0 (4.52).

*Ethyl 4-(4-((5-cyano-2-hydroxy-4-methyl-6-oxo-1-phenyl-1,6-dihydropyridin-3-yl)diazenyl)phenyl)-6-methyl-2-oxo-1,2,3,4-tetrahydropyrimidine-5-carboxylate (**4**).* Dark orange powder, 70%, m.p. 243–244 °C; ATR-FTIR ($\nu$/$cm^{-1}$): 3248 (NH), 2219 (CN), 1678 (CO), 1629 (CO), 1503 (NH). $^1$H NMR (400 MHz, DMSO-$d_6$, $\delta$/ppm): 1.11 (3H, t, $J$ = 7.2 Hz, $COOCH_2C\underline{H_3}$), 2.26 (3H, s, $CH_3$ DHPM), 2.62 (3H, s, $CH_3$ Py), 4.00 (2H, q, $J$ = 6.8 Hz, $COOC\underline{H_2}CH_3$), 5.17 (1H, d, $J$ = 2.4 Hz, C-H), 7.28–7.34 (4H, m, Ar), 7.46–7.69 (5H, m, Phenyl substituent), 7.76 (1H, s, NH), 9.23 (1H, s, NH), 14.49 (1H, s, NH hydrazone). $^{13}$C NMR (200 MHz, DMSO-$d_6$, $\delta$/ppm): 14.58 ($COOCH_2\underline{C}H_3$), 16.95 ($CH_3$, Py), 18.27 ($CH_3$, DHPM), 54.04 (C-H), 59.72 ($COO\underline{C}H_2CH_3$), 99.40 ($\underline{C}$–$COOCH_2CH_3$), 101.20 (CN), 115.58 ($\underline{C}$–CN), 118.12 (Ar), 123.88 (C=N, Py), 128.16 (Ar), 129.10 (Ar, Phenyl substituent), 129.32 (Ar, Phenyl substituent), 129.43 (Ar, Phenyl substituent), 134.59 (Ar, Phenyl substituent), 140.79 (Ar), 144.19 (Ar), 149.14 ($\underline{C}$–$CH_3$, DHPM), 152.45 (CO, DHPM), 160.18 (Py), 160.65 (CO, Py), 161.11 (CO, Py), 165.73 ($\underline{C}OOCH_2CH_3$); Anal. Calcd for $C_{27}H_{24}N_6O_5$ (512.52): C, 63.27; H, 4.72; N, 16.40%; Found: C, 63.49; H, 4.95; N, 16.51%; ESI-MS m/z calc. 512.18, found (negative mode): 511.18 $[M–H]^-$, found (positive mode): 513.17 $[M+H]^+$; UV-Vis (EtOH) ($\lambda_{max}$/nm (log ε/$mol^{-1}dm^3cm^{-1}$)): 443.0 (4.58).

*Ethyl 4-(4-((5-cyano-2-hydroxy-6-oxo-4-phenyl-1,6-dihydropyridin-3-yl)diazenyl)phenyl)-6-methyl-2-oxo-1,2,3,4-tetrahydropyrimidine-5-carboxylate (**5**).* Dark orange powder; yield 61%; m.p. 275-276 °C; ATR-FTIR ($\nu$/$cm^{-1}$): 3405 (NH), 3210 (NH), 2229 (CN), 1693 (CO), 1652 (CO), 1505 (NH). $^1$H NMR (400 MHz, DMSO-$d_6$, $\delta$/ppm): 1.07 (3H, t, $J$ = 7,2 Hz, $COOCH_2C\underline{H_3}$), 2.24 (3H, s, $CH_3$ DHPM), 3.97 (2H, q, $J$ = 8 Hz, $COOC\underline{H_2}CH_3$), 5.11 (1H, d, $J$ = 3,2 Hz, C-H), 7.20–7.26 (4H, m, Ar–H), 7.51–7.59 (5H, m, Phenyl substituent), 7.69 (1H, s, NH), 9.18 (1H, s, NH),

12.19 (1H, s, NH pyrimidine), 14.60 (1H, s, NH hydrazone). $^{13}$C NMR (200 MHz, DMSO-$d_6$, $\delta$/ppm): 14.54 ($COOCH_2\underline{C}H_3$), 18.29 ($CH_3$, DHPM), 54.04 (C–H), 59.68 ($COO\underline{C}H_2CH_3$), 99.23 ($\underline{C}$-$COOCH_2CH_3$), 100.64 (CN), 115.73 ($\underline{C}$–CN), 117.65 (Ar), 124.05 (C=N, Py), 128.11 (Ar), 128.32 (Ar), 129.91 (Ar, Phenyl substituent), 130.47 (Ar, Phenyl substituent), 133.35 (Ar, Phenyl substituent), 140.73 (Ar), 144.02 (Ar), 149.15 ($\underline{C}$–$CH_3$, DHPM), 152.35 (CO, DHPM), 161.35 (Py), 161.46 (CO, Py), 162.16 (CO, Py), 165.69 ($\underline{C}OOCH_2CH_3$); Anal. Calcd for $C_{26}H_{22}N_6O_5$ (498.49): C, 62.64; H, 4.45; N, 16.86%; Found: C, 62.80; H, 4.66; N, 16.91%; ESI-MS m/z calc. 498.17, found (negative mode): 497.19 $[M–H]^-$. UV-Vis (EtOH) ($\lambda_{max}$/nm (log $\varepsilon$/mol$^{-1}$dm$^3$cm$^{-1}$)): 442.5 (4.58).

*Ethyl 4-(4-((5-carbamoyl-2-hydroxy-4-methyl-6-oxo-1,6-dihydropyridin-3-yl)diazenyl)phenyl)-6-methyl-2-oxo-1,2,3,4-tetrahydropyrimidine-5-carboxylate (**6**).* Orange solid; yield 61%; m.p. 201-203 °C. ATR-FTIR ($\nu$/cm$^{-1}$): 3248 (NH), 1684 (CO), 1648 (CO), 1513 (NH). $^1$H NMR (400 MHz, DMSO-$d_6$, $\delta$/ppm): 1.11 (3H, t, $J$ = 7 Hz, $COOCH_2C\underline{H}_3$), 2.22 (3H, s, $CH_3$ DHPM), 2.26 (3H, s, $CH_3$ DHPM), 3.99 (2H, q, $J$ = 7 Hz, $COO\underline{H}_2CH_3$), 5.15 (1H, d, $J$ = 2.4 Hz, C–H), 7.28 (2H, d, $J$ = 8.2 Hz, Ar–H), 7.50–7.52 (3H, m, Ar–H and $CON\underline{H}_2$), 7.69 (1H, s, $CON\underline{H}_2$), 7.79 (1H, s, NH), 9.22 (1H, s, NH), 11.66 (1H, s, NH Py), 14.23 (1 H, s, NH hydrazone). $^{13}$C NMR (200 MHz, DMSO-$d_6$, $\delta$/ppm): 14.59 ($COOCH_2\underline{C}H_3$), 14.75 ($CH_3$, Py), 18.26 ($CH_3$, DHPM), 54.01 (C-H), 59.70 ($COO\underline{C}H_2CH_3$), 99.57 ($\underline{C}$-$COOCH_2CH_3$), 116.49 ($\underline{C}$–CN), 116.69 (Ar), 126.23 (C=N, Py), 128.06 (Ar), 141.38 (Ar), 145.78 (Ar), 148.94 ($\underline{C}$–$CH_3$, DHPM), 152.51 (CO, DHPM), 162.19 (Py), 162.22 (CO, Py), 162.42 (CO, Py), 165.76 ($\underline{C}OOCH_2CH_3$), 166.81 ($CONH_2$); Anal. Calcd for $C_{21}H_{22}N_6O_6$ (454.44): C, 55.50; H, 4.88; N, 18.49%; Found: C, 55.69; H, 4.92; N, 18.63%; ESI-MS m/z calc. 454.16, found (negative mode): 453.19 $[M–H]^-$, found (positive mode): 454.99

263 $[M+H]^+$, found (positive mode): 477.11 $[M+Na]^+$; UV-Vis (EtOH) ($\lambda_{max}$/nm (log
264 $\varepsilon$/mol$^{-1}$dm$^3$cm$^{-1}$)): 428.5 (4.60).
265 *Ethyl 4-(4-((2-hydroxy-4-methyl-6-oxo-5-pyridinium-1,6-dihydropyridin-3-yl)diazenyl)phenyl)-6-*
266 *methyl-2-oxo-1,2,3,4-tetrahydropyrimidine-5-carboxylate (**7**).* Red powder; yield 61%; m.p. 230-
267 232; ATR-FTIR ($\nu$/cm$^{-1}$): 3382 (NH), 3233 (NH), 1690 (CO), 1616 (CO); $^1$H NMR (400 MHz,
268 DMSO-$d_6$, $\delta$/ppm): 1.11 (3H, t, $J$ = 7 Hz, $COOCH_2C\underline{H}_3$), 2.14 (3H, s, $CH_3$ Py), 2.25 (3H, s, $CH_3$
269 DHPM), 3.99 (2H, q, $J$ = 7 Hz, $COOC\underline{H}_2CH_3$), 5.14 (1H, s, C–H), 7.24 (2H, d, $J$ = 8 Hz, Ar–H),
270 7.46 (2H, d, $J$ = 8 Hz, Ar–H), 7.74 (1H, s, NH), 8.23 (2H, t, $J$ = 6.8 Hz, Pyridinium substituent),
271 8.69 (1H, t, $J$ = 7.6 Hz, Pyridinium substituent), 9.06 (2H, d, $J$ = 5.6 Hz, Pyridinium substituent),
272 9.20 (1H, s, NH), 10.47 (1H, s, Py); $^{13}$C NMR (200 MHz, DMSO-$d_6$, $\delta$/ppm): 14.59
273 ($COOCH_2\underline{C}H_3$), 18.26 ($CH_3$, DHPM), 54.20 (C–H), 59.67 ($COO\underline{C}H_2CH_3$), 99.78 ($\underline{C}$–
274 $COOCH_2CH_3$), 127.35 (Ar), 128.31 (C=N, Py), 148.71 (Ar, Pyridinium substituent), 152.59 (CO,
275 DHPM), 165.85 (CO, $COOCH_2CH_3$); $^1$H NMR (400 MHz, $CF_3COOD$, $\delta$/ppm): 1.34 (3H, t, $J$ = 7
276 Hz, $COOCH_2C\underline{H}_3$), 2.46 (3H, s, $CH_3$ Py), 4.32 (2H, q, $J$ = 7 Hz, $COOC\underline{H}_2CH_3$), 5.76 (1H, s, C–
277 H), 7.65 (2H, d, $J$ = 8.8 Hz, Ar-H), 7.75 (2H, d, $J$ = 8.4 Hz, Ar–H), 8.38 (2H, d, $J$ = 7 Hz,
278 Pyridinium substituent), 8.87–8.91 (3H, m, Pyridinium substituent), 10.01 (1H, s, NH), 10.82 (1H,
279 s, NH pyrimidine), 15.02 (1H, s, NH hydrazone); $^{13}$C NMR (200 MHz, $CF_3COOD$, $\delta$/ppm): 14.46
280 ($COOCH_2\underline{C}H_3$), 14.68 ($CH_3$, Py), 57.72 (C–H), 65.25 ($COO\underline{C}H_2CH_3$), 104.58 (C–$COOCH_2CH_3$),
281 123.70 ($\underline{C}$–CN), 128.32 (C=N, Py), 131.21 (Ar, Pyridinium substituent), 131.53 (Ar, DHPM),
282 143.03 (Ar, DHPM), 145.69 (Ar, DHPM), 149.40 (Ar, Pyridinium substituent), 150.94 ($\underline{C}$–$CH_3$,
283 DHPM), 155.64 (CO, DHPM), 163.04 (Py), 170.64 (CO, $COOCH_2CH_3$); Anal. Calcd for
284 $C_{25}H_{25}N_6O_5$ (489.50): C, 61.34; H, 5.15; N, 17.17%; Found: C, 61.51; H, 5.58; N, 17.35%; ESI-

MS m/z calc. 498.19, found (positive mode) 489.29 [$M^+$]; UV-Vis (EtOH) ($\lambda_{max}$/nm (log $\varepsilon$/mol$^{-1}$dm$^3$cm$^{-1}$)): 428.0 (4.60).

*2.3. Computational details*

DFT calculations of investigated dyes were performed using Gaussian 09 program package [30] with B3LYP/6-311++G(d,p) method. The default convergence criteria were used without any constraint on the geometry. The stability of the optimized geometry was checked by frequency calculations, which gave real values for all the obtained frequencies. Optimized geometry data were used in the calculations of IR and NMR spectra as well as energies of frontier molecular orbitals (FMO).

The harmonic frequencies were calculated with B3LYP/6-311++G(d,p) method and then scaled by 0.968 [31]. The assignments of the calculated wavenumbers were utilized by the animation option of GaussView 5.0 graphical interface [32] from Gaussian programs, which performed a visual presentation of the feature of vibration modes.

The nuclear magnetic resonance (NMR) chemical shifts calculations were accomplished with Gauge-Independent Atomic Orbital (GIAO) method, at the same level of theory in DMSO. The solvent effect was inducted with CPCM (Conductor Polarizable Continuum Model). In attempt to correct the large deviation between experimental and calculated $^1$H NMR shift for hydrogen in N-H groups in DMSO-$d_6$, as solvent, three DMSO molecules were explicitly added in the position that allowed the formation of hydrogen bonds in molecule. The $^1$H and $^{13}$C isotropic chemical shifts are presented in relation to the corresponding values for TMS. The energies of frontier molecular orbitals (FMO) and molecular electrostatic potential (MEP) maps analyses helped to explain reactivity of dye molecules.

The quantum chemical descriptors, such as the energy of the highest occupied molecular orbital ($E_{HOMO}$), the energy of the lowest unoccupied molecular orbital ($E_{LUMO}$), HOMO-LUMO energy gap ($E_{GAP}$), ionization energy ($I$), electron affinity ($A$), absolute hardness ($\eta$), absolute softness ($\sigma$), optical softness ($\sigma_o$), global softness ($S$), absolute electronegativity ($\chi$), chemical potential ($CP$), electrophilicity index ($\omega$), nucleophilicity index ($N$) and additional electronic charges ($\Delta N_{max}$) were calculated in water to investigate biological reactivity. The $E_{HOMO}$ and $E_{LUMO}$ were taken directly from the calculation, while other QCDs were estimated by equations [33] given in Supplementary material.

2.4. *Antioxidant activity*

The antioxidant activity of investigated dyes was determined by the ABTS radical-scavenging assay [34]. A stock solution of the $ABTS^{\bullet+}$ radical cation was prepared in the reaction of ABTS (4.912 mL, 7 mM in phosphate-buffered saline (PBS)) and potassium persulfate (0.088 mL, 140 mM in distilled water). After 16 h of incubation in the dark, the stock solution was diluted with methanol until absorbance recorded at 734 nm was 0.700 ± 0.02. Subsequently, 20 μL of the methanolic dye solutions (2 mM) were mixed with 2 mL of the ABTS radical solution, shaken and stored in the dark for 10 min. Afterwards the absorbance was measured at 734 nm. Each test was done in triplicate. The inhibition percentage of $ABTS^{\bullet+}$ was calculated using the formula:

Inhibition (%) = ($Ac$–$As$) / $Ac$ × 100, where Ac is the absorbance of the control solution (20 μL of methanol in 2 mL of ABTS solution) and As is the absorbance of the sample solution. Ascorbic acid was used as a standard antioxidant. The antioxidant ability of the most promising candidates **5**, **6** and **7** was further evaluated by determination of the $IC_{50}$ values. The methanolic solutions of selected dyes and ascorbic acid were prepared at concentration ranging from 2 mM do 0.5 mM,

and obtained $IC_{50}$ were compared. The tests were performed in triplicate. Resulting $IC_{50}$ values are presented as means with standard deviation (±SD) from three experiments (n = 3).

*2.5. In vitro cytotoxic activity*

The cytotoxic activity of seven novel dyes **1**–**7** and their precursor **B2** was examined against three human cancer cell lines: prostate adenocarcinoma PC-3, lung carcinoma A549, and chronic myelogenous leukemia K562, as well as on human normal lung fibroblasts MRC-5. The cytotoxic evaluation of all compounds against normal cells MRC-5 was carried out to explore the toxicity and selectivity of the tested compounds. All tested cell lines were obtained from the American Type Culture Collection (Manassas, VA, USA). Stock solutions of the compounds were made in a dimethyl sulfoxide at the concentration of 10 mM. All tested cell lines were cultured in a RPMI-1640 nutrient medium which contained 2 mM L-glutamine, 100 μg/mL streptomycin, 100 IU/mL penicillin, 10% heat-inactivated (56 °C) fetal bovine serum and 25 mM HEPES, adjusted to pH 7.2 with a bicarbonate solution. PC-3 (5,000 cells per well), A549 (5,000 cells per well), and MRC-5 cells (5,000 cells per well) were seeded into 96-well microtiter plates and the next day five different concentrations of the compounds were added to the cells. K562 cells (5,000 cells per well) were seeded 2 h before the addition of the compounds. The nutrient medium was added to the control cells. The CDDP (cisplatin) was used as a standard reference drug. The cell survival was measured by MTT (3-(4,5-dimethylthiazol-2-yl)-2,5-diphenyltetrazolium bromide) colorimetric assay after 72 h incubation of cells with compounds, according to the standard protocol firstly described by Mosmann [35], and which was modified by Ohno and Abe [36]. The experiments were repeated three times and performed in triplicate.

*2.4. Cell cycle analysis by flow cytometry*

Chronic myelogenous leukemia K562 cells were seeded into 6-well plates, and 2 hours later the cells were treated with $2IC_{50}$ concentration of the compound **5**. The control K562 cells were cultured in a RPMI-1640 nutrient medium, as previously described. After 24 h treatment, the control cells and the cells treated with compound **5** were harvested, washed in PBS and fixed in 70% ethanol on ice, according to standard protocol [37]. The cell samples were stored one week on -20°C. Afterwards, the ethanol was removed and cells were washed in PBS. The cells were treated with RNase A for 30 min at 37°C, and then stained with propidium iodide. The percentage of K562 cells in the subG1, G1, S and G2/M phases of the cell cycle were determined using a BD FACSCalibur flow cytometer. The analyses of acquired data (10,000 events collected for each gated cell sample) were done using a CELLQuest software.

### *2.5. In silico assessment of physicochemical and ADME properties*

The molecular structures of hydrazones **1–7** and zwitter ionic form **7a** (Supplementary material, Figure S24) were converted into SMILES database using ChemDraw Ultra 12.0. Then, these SMILES were inserted in SwissADME [38] website to calculate the physicochemical descriptors, pharmacokinetic properties, ADME parameters and medicinal chemistry data. In addition, the physicochemical descriptors were estimated by program Vega 22 version 2.4 [39] from previously optimized geometries with B3LYP/6-311++G(d,p) method.

## 3. Results and discussion

### *3.1. Synthesis*

Novel azo dyes **1–7** were synthesized *via* classical diazo coupling reactions between diazonium salt, formed by diazotization of **B2**, and corresponding 6-hydroxy-2-pyridone **P1–7** (Figure 1). The obtained azo compounds were isolated in a good yield, and their structures were confirmed by ATR-FTIR, $^{1}$H NMR,$^{13}$C NMR, ESI-MS, UV–Vis spectra and elemental analysis. The

synthesized DHPM-azo pyridone dyes **1–7**, contain hydroxy group in the *ortho*- position to the azo linkage, enabling intramolecular proton transfer, and thus the existence of the azo and the hydrazone tautomeric forms (Figure 1) [40].

The ATR-FTIR and NMR data of novel dyes **1–6** suggest the existence of the hydrazone tautomeric form (Figure 1) in the solid state, as well as, in the DMSO-$d_6$ solution. The stretching vibrations of the carbonyl groups appear in the ATR-FTIR spectra in the region of 1709–1616 $cm^{-1}$. The N-H stretching vibrations of the hydrazone group appear in the region of 3210–3296 $cm^{-1}$. Additional confirmation of the presence of the hydrazone form is intensive band appearing in the region of 1514–1503 $cm^{-1}$ which is ascribed to mutual stretching of C=N and bending of N–H vibrations. The $^{1}H$ NMR spectra of dyes **1–6**, obtained in DMSO-$d_6$ solution, contain the signal of the hydrazone N–H group in the range of 14.23–14.62 ppm. The $^{13}C$ NMR spectra confirmed the presence of hydrazone form, which is evidenced by signals of two carbonyl carbons, originating from pyridone moiety, in the range of 160.65–162.22 ppm (Figure 1, C6) and 161.11–164.20 ppm (Figure 1, C2).

Exceptionally, dye **7** is found to be in a deprotonated hydrazone form (zwitter ionic form) in a solid state, as well as in DMSO-$d_6$ solution (Figure S36, Supplementary material, Structure **7a**). Since coupling reactions have been performed under the alkaline conditions, dye **7** can be simply deprotonated during the synthesis. Namely, $^{1}H$ NMR spectrum of **7**, in DMSO-$d_6$ solution, did not contain the signal of the proton resonance of hydrazone –NH group, but $^{13}C$ NMR analysis detected signal assigned to C5=N at 128.31 ppm. Also, ATR-FTIR analysis confirmed zwitter ionic structure in solid state, since N–H bending vibrations, attributed to the hydrazone –NH group, have not been presented in the spectrum. However, the existence of hydrazone form is confirmed by NMR analysis in $CF_3COOD$ solution. The signal of low intensity at 15.03 ppm, in $^{1}H$ NMR

spectrum, was ascribed to the N–H proton resonance of the hydrazone –NH group [41], and signal at 128.32 ppm, in $^{13}$C NMR spectrum, was ascribed to C5=N.

Nevertheless, the ESI-MS spectra of the dyes **1–7** showed the molecular ion peaks at the m/z values corresponding to the molecular weight of the investigated dyes.

The UV-Vis spectra of the studied molecules in ethanol are shown in Figure 2. The obtained absorption spectra suggest the existence of hydrazone tautomeric form in case of all investigated dyes [16-18,41,42].

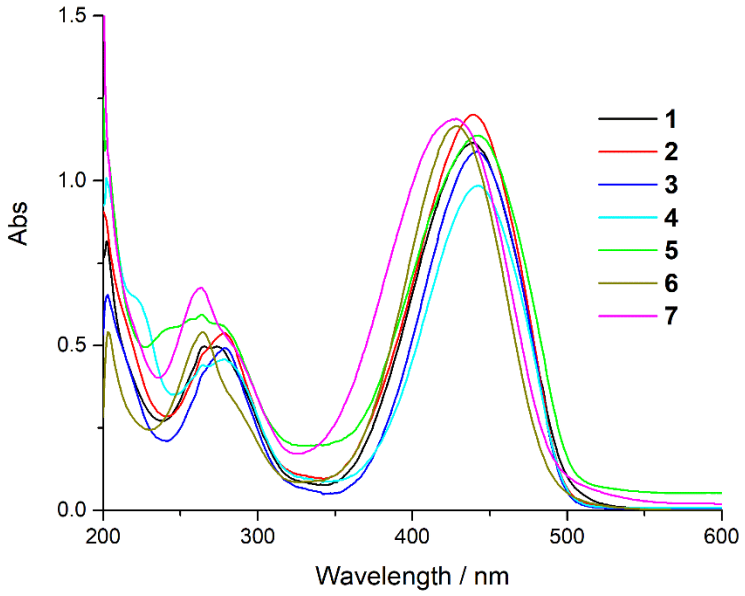


Figure 2. UV-Vis spectra of dyes **1**–**7** in ethanol.

It can be observed in Figure 2 that different substituents at the N atom, of the pyridone ring, in case of dyes **1**–**4**, do not affect significantly the positions of the UV–Vis absorption maxima [43]. Also, the replacement of the methyl group, on the C4 atom of the pyridone ring, with phenyl group, in case of dye **5**, does not make a notable difference in the position of the absorption maximum, comparing to dyes **1**–**4**. However, in case of dye **6**, the replacement of the 3-cyano group, on the pyridone moiety, with a weaker electron-accepting 3-amido group, causes a hypsochromic shift of the absorption maximum [44]. Dye **7** carrying the pyridinium ring on the pyridone moiety has

absorption maximum at the lowest wavelength comparing to dyes **1**–**6**. This behavior is assumed to be the consequence of the planarity disruption of the molecule which causes hypsochromic shift of the absorption maximum.

*3.2.Conformational analysis*

The calculated energy data of possible tautomeric forms confirm that the most stable form of the investigated dyes is hydrazone one for dyes **1–6,** and deprotonated hydrazone (zwitter ion) for dye **7**. The optimized geometries of the most stable conformers of dye **1** obtained with B3LYP method are presented in Figure 3. It can be seen that the phenylazo pyridone part of molecule is planar, while the DHPM group is orthogonal to that plane, preventing electron delocalization between these two parts of the molecule. The largest conformational difference in the molecule results from the rotation of the DHPM group around the C14–C20 bond. The B3LYP/6-31+G(d) calculation in gas phase showed that the energy barrier for this rotation is ~2.0 kcal/mol and the rotation produces two conformers with almost identical energies (Figure 4). The overall process can be also done by changing the torsion angle around C9–N1 bond but the rotation energy for this process is significantly higher, ~6 kcal/mol, which is in line with our previously published results for same bond in similar compound (Supplementary material, Figure S37) [45].

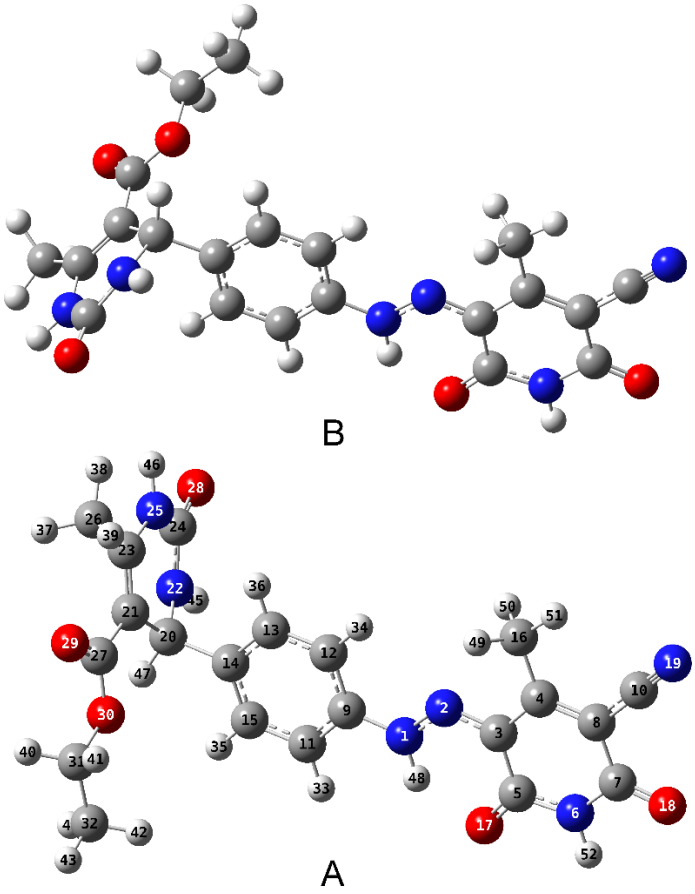


Figure 3. The optimized geometries of the most stable conformers of dye **1** obtained with B3LYP method with used atoms numeration.

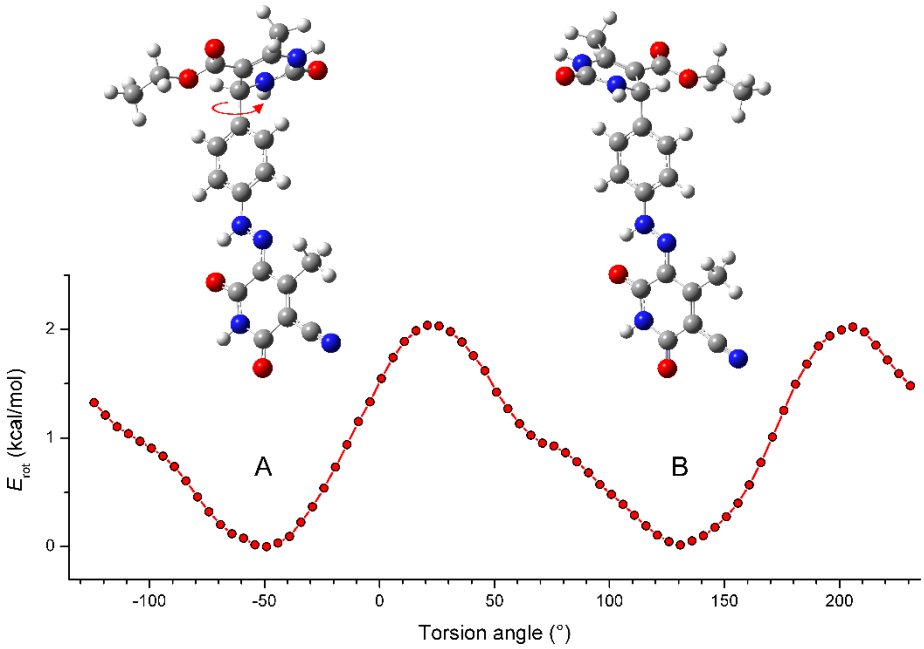


Figure 4. Potential energy surface for the rotation of the DHPM group around the C14–C20 bond of dye **1**.

*3.3. Vibrational analysis*

The vibration frequencies of hydrazone tautomer of dye **1** were calculated with B3LYP/6-311++G(d,p) method and the most characteristic of them are compared with experimental ones. The good correlation confirmed the hydrazone form in solid state. The visual comparison of the experimental and calculated spectrum is presented in Figure 5. The calculated and experimental vibrational frequencies of dye **1** are presented in Table 1, and numeration of the dye is given in Figure 3.

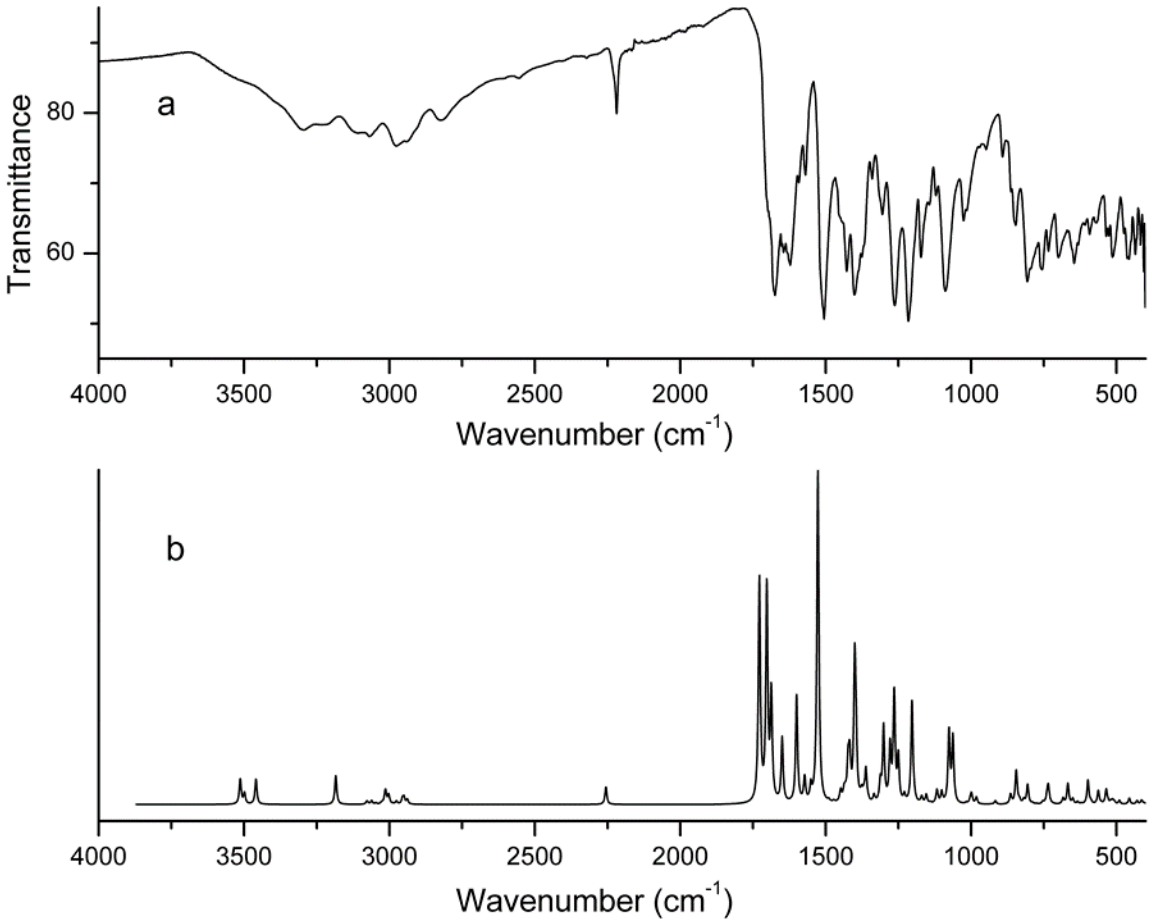


Figure 5. The experimental (a) and calculated (b) IR spectra of dye **1**.

Table 1. The observed FT-IR and calculated (B3LYP/6-311++G(d,p)) frequencies for hydrazone tautomer of dye **1** [harmonic frequency ($cm^{-1}$), $IR_{int}$ (K $mmol^{-1}$)].

| Mode no. | IR exp $cm^{-1}$ | Unscaled B3LYP | Scaled B3LYP | $IR_{Int}$[a] | Assignments |
|---|---|---|---|---|---|
| 150 | 3450 | 3630 | 3514 | 86.75 | νN25–H46 |
| 149 | 3430 | 3614 | 3498 | 37.9 | νN22–H45 |
| 148 | 3296 | 3574 | 3460 | 87.46 | νN6–H52 |
| 147 | 3211 | 3290 | 3185 | 99.00 | νN1–H48 |
| 144 | 3114 | 3178 | 3076 | 7.45 | $\nu_{sym}$CH |
| 143 | 2977 | 3147 | 3046 | 12.1 | $\nu_{asym}$CH |
| 130 | 2219 | 2330 | 2255 | 59.5 | νCN |
| 129 | 1700 | 1785 | 1728 | 773.79 | νC24=O28 |
| 128 | 1674 | 1759 | 1703 | 744.8 | νC7=O18 |
| 127 | 1640 | 1743 | 1687 | 363.33 | νC27=O29 |

| | | | | | |
|---|---|---|---|---|---|
| 126 | 1622 | 1704 | 1649 | 233.25 | νC5=O17 |
| 123 | 1570 | 1624 | 1572 | 184.8 | νC=C + βN1–H48 |
| 122 | 1506 | 1602 | 1551 | 1163.83 | νC3=N2 + βN1–H48 |
| 121 | 1450 | 1577 | 1527 | 51.96 | νC4=C8 + νN1–N2 |
| 117 | 1428 | 1496 | 1448 | 36.56 | βN25–H46 |
| 112 | 1401 | 1470 | 1423 | 119.3 | βN22–H45 + βCH |
| 109 | 1390 | 1447 | 1401 | 449.0 | βN1–H48 + βN6–H52 |
| 68 | 847 | 872 | 844 | 66.15 | γN1–H48 |
| 55 | 699 | 706 | 683 | 19.44 | βC5=O17 + βC7=O18 |
| 54 | 646 | 689 | 667 | 71.4 | γN6–H52 |
| 50 | 592 | 618 | 598 | 83.00 | γN22–H45 + γN25–H46 |

[a]$IR_{Int}$ – IR intensity; K $mmol^{-1}$; ν – stretching; $\nu_{sym}$ symmetric stretching; $\nu_{asym}$ – asymmetric stretching; β – in-plane bending; γ – out-of-plane bending.

Two broad bands at 3430 and 3450 $cm^{-1}$ in experimental spectrum are assigned to symmetric and asymmetric stretching vibrations of two N22−H45 and N25−H46 groups of DHMP moiety, which correlate with 3498 and 3514 $cm^{-1}$ in calculated spectrum. For hydrazone form of dye **1**, the most important are two weak bands at 3211 and 3296 $cm^{-1}$, which belong to stretching vibrations of N1−H48 and N6−H52 bonds of hydrazone and pyridone groups, respectively. These assignments are supported by scaled theoretical values 3185 and 3460 $cm^{-1}$ (B3LYP mode nos. 147 and 148), respectively, as well as with literature data. The bands centered at 2977 and 3114 $cm^{-1}$ in FT-IR are assigned to aromatic asymmetric and symmetric C−H stretching vibrations. It can be seen from Table 1 that in-plane bending vibrations of N1−H48 and N6−H52 are at 1390 $cm^{-1}$ and counterpart in calculated spectrum is at 1401 $cm^{-1}$. The medium strong peaks at 646 and 847 $cm^{-1}$ are ascribed to out-of-plane bending vibrations of N6−H52 and N1−H48 bonds, respectively. The band characteristic for stretching vibrations of CN group at 2219 $cm^{-1}$ correlate well with calculated value 2255 $cm^{-1}$.

The stretching bands of polar carbonyl groups C5=O17 and C7=O18 of pyridone and C24=O28 of DHMP moieties are at 1622, 1674 and 1700 $cm^{-1}$, respectively, and correlate well with calculated values 1649, 1703 and 1728 $cm^{-1}$ (B3LYP mode nos. 126, 128 and 129). Vibrational

mode of C27=O29 of ethoxycarbonyl group is at 1640 $cm^{-1}$ which is in accordance with the theoretically scaled frequencies at 1687 $cm^{-1}$. The band appearing at 699 $cm^{-1}$ in FT-IR spectrum originated from in-plane bending vibrations of C5=O17 and C7=O18 of pyridone ring, and the corresponding scaled calculated value is 683 $cm^{-1}$. The existence of stretching and bending bands of carbonyl groups in FT-IR spectrum and their correlation with calculated values confirmed the hydrazone tautomer of dye **1**. Additional evidence of hydrazone tautomer is stretching N1–N2 and C3=N2 group vibrations appeared as intensive sharp bands at 1450 and 1506 $cm^{-1}$ in FT-IR spectrum. The band appearing at 1527 $cm^{-1}$ has contributions from the N1−N2 and C4=C8 stretching vibrations in calculated spectrum. The calculated stretching vibrations of C3=N2 group is coupled with in-plane-bending vibrations of N1−H48 at 1551 $cm^{-1}$. The out-of-plane bending vibrations of four N−H groups are in the low-frequency region at 592–847 and 598–844 $cm^{-1}$ in experimental and calculated spectra, respectively. From Table 1 it is evident that experimental data correlate well with the calculated data of hydrazone tautomer of **1**.

*3.4. NMR spectral analysis*

Powerful confirmation of the tautomeric structure of dyes **1**–**7** results from the analysis of their NMR spectra. In this part, analysis of the most significant $^{1}H$ and $^{13}C$ NMR chemical shifts of dye **1** is done in attempt to confirm its hydrazone tautomeric form. The calculated and experimental $^{1}H$ and $^{13}C$ NMR chemical shifts are presented in Table 2. The recorded $^{1}H$ and $^{13}C$ NMR spectra of **1** in DMSO-$d_6$ are shown in Figure S1 and S2 (Supplementary material).

In the experimental $^{1}H$ NMR spectrum, the chemical shift values for hydrogen of ethyl group are 1.1 and 3.99 ppm. Signals for two methyl groups of DHMP and pyridone moieties are at 2.26 and 2.51 ppm, respectively. These chemical shifts correlate well with calculated values in aliphatic region 1.14–4.0 ppm, with respect to TMS, in DMSO solution by B3LYP/6-311++G(d,p) method.

The experimental peaks at 7.33–7.64 ppm are originating from aromatic hydrogen atoms. The calculated values of these peaks are in the region 7.49–8.23 ppm. Two signals of hydrogen H45 and H46 of NH groups of DHMP appear at 7.79 and 9.25 ppm in experimental spectrum. They are determined at 9.34 and 10.74 ppm in calculated spectrum. The most significant signals for hydrazone tautomer of dye **1** are signals of H52 and H48 belonging to pyridone and hydrazone NH groups, at 12.02 and 14.58 ppm. The calculated values of these signals are at 13.03 and 14.74 ppm.

The most significant signals for hydrazone tautomer in experimental $^{13}C$ NMR spectrum of dye **1** are signals of two carbon atoms C5 and C7 of pyridone ring carbonyl groups, at 160.95 and 161.32 ppm, respectively. Counterparts of these signals in calculated spectrum are at 167.46 and 168.86 ppm. Signal at 124.04 ppm in experimental spectrum is assigned to carbon atom of C3=N2 group with calculated value of 130.84 ppm. The appearance of these signals in experimental spectrum is in a good correlation with the calculated chemical shifts for hydrazone tautomer of dye **1** which is a proof of the hydrazone structure. From Table 2 is evident that experimental and calculated chemical shifts correlate very well.

Table 2. Experimental and calculated $^{1}H$ NMR and $^{13}C$ NMR chemical shifts of dye **1** in DMSO (with respect to TMS, atom positions are numbered as in Figure 3) [chemical shift (ppm)].

| No. | Calc. | Exp. | No. | Calc. | Exp. |
|---|---|---|---|---|---|
| 48-H | 14.74 | 14.58 | 4-C | 175.46 | 165.72 |
| 52-H | 13.03 | 12.02 | 27-C | 173.56 | 161.97 |
| 46-H | 10.74 | 9.25 | 7-C | 168.86 | 161.32 |
| 45-H | 9.34 | 7.79 | 5-C | 167.46 | 160.95 |
| 34-H | 8.23 | 7.64 | 23-C | 163.42 | 152.45 |
| 36-H | 7.69 | 7.33 | 24-C | 158.25 | 149.13 |
| 35-H | 7.68 | 7.33 | 14-C | 153.91 | 144.04 |
| 33-H | 7.49 | 7.64 | 9-C | 149.08 | 140.73 |
| 47-H | 5.38 | 5.17 | 13-C | 137.05 | 128.17 |
| 40-H | 4.00 | 3.99 | 15-C | 136.82 | 128.17 |

| | | | | | |
|---|---|---|---|---|---|
| 41-H | 3.77 | 3.99 | 3-C | 130.84 | 124.04 |
| 50-H | 2.68 | 2.51 | 11-C | 127.08 | 115.59 |
| 49-H | 2.63 | 2.51 | 10-C | 123.81 | 117.95 |
| 39-H | 2.61 | 2.26 | 12-C | 123.11 | 115.59 |
| 37-H | 2.46 | 2.26 | 21-C | 104.60 | 101.09 |
| 51-H | 2.45 | 2.51 | 8-C | 104.34 | 99.38 |
| 38-H | 2.27 | 2.26 | 31-C | 66.56 | 59.73 |
| 44-H | 1.37 | 1.1 | 20-C | 62.08 | 54.04 |
| 43-H | 1.15 | 1.1 | 26-C | 24.01 | 18.27 |
| 42-H | 1.14 | 1.1 | 16-C | 21.58 | 16.92 |
| | | | 32-C | 15.55 | 14.58 |

### *3.4. Calculated MEP maps of the investigated dyes*

In strive to reveal (re)activity toward electrophilic or nucleophilic attack for dye molecules, the MEP maps on the B3LYP/6-311++G(d,p) optimized geometries are calculated. From Figure S38, Supplementary material, it can be concluded that dye molecules have three possible sites for electrophilic attack, according to negative regions, which exist around the oxygen atoms of carbonyl groups of pyridone ring and nitrile group. Contrary, the possible sites for nucleophilic attack are maximum positive regions spread around hydrogen atoms belonging to two N-H groups of DHMP ring.

### *3.5. Calculated quantum chemical descriptors for investigated dyes*

The massive efforts and substantial financial resources are being invested in studies of biological (re)activity of the molecules. However, computational chemistry may help in such researches by calculation of the biological reactivity of promising molecules [33]. In this purpose, quantum chemical descriptors (QCDs) for investigated dyes **1–7** were calculated in water, employing equations [33] given in Supplementary material (Equations S1-S12). The calculations of QCDs have been performed in water, considering that bioassays were conducted in the aqueous solution of the nutrient medium and other chemicals. Also, determination of QCDs in water can show the

general tendency of biological (re)activity [46] for investigated molecules. In previous publications [33, 47], it has been explained how QCDs affect biological reactivity. The calculated QCDs for the studied molecules **1–7** are given in Table S1, Supplementary material. Also, bearing in mind that dye **7** is likely to be in a zwitter ionic form, the profiling was conducted for both structures, hydrazone (**7**) and zwitter ion (**7a**). The biological reactivity of related dyes **1–7**, regarding QCDs is given in Table 3.

Table 3. The biological reactivity of investigated dyes regarding QCDs

| | Biological reactivity |
|---|---|
| According to $E_{HOMO}$ | 7a> 6 > 3 > 2 > 4 > 1 > 5 > 7 |
| According to $E_{LUMO}$ | 5 > 7 > 1 > 4 > 2 > 3 > 6 > 7a |
| According to $E_{GAP}$ | 7a > 5 > 1 > 4 = 2 > 3 > 6 = 7 |
| According to I | 7a > 6 > 3 > 2 > 4 > 1 > 5 > 7 |
| According to A | 7a > 6 > 3 > 2 > 4 > 7 > 1 > 5 |
| According to η | 7a > 5 > 1 > 4 > 2 > 3 > 7 > 6 |
| According to σ, $\sigma_o$, S | 7a > 5 > 1 > 2 > 4 > 3 > 6 > 7 |
| According to χ | 5 > 7 > 1> 4 > 2 > 3 > 6 > 7a |
| According to CP | 7a > 6 > 3 > 2 > 4 > 1> 7 > 5 |
| According to ω, N, $\Delta N_{max}$ | 7a > 6 > 3 > 2 > 4 > 7 > 1 > 5 |

Above results show that there is no solely sequence of reactivity, but dye molecules **7a** and **5** appear to be more biologically reactive comparing to others. It is important to note that QCDs show just the tendency of biological reactivity, and this reactivity can be changed with respect to the structure of biological target [47,48].

*3.6. Antioxidant activity*

Antioxidant properties of the investigated dyes have been evaluated using the ABTS assay. The scavenging activity of dyes was compared to the activity of ascorbic acid (Figure 6a). The results have shown variable activity of the compounds, indicating that substituents on the pyridone moiety affect the oxidant ability of the molecules. Namely, 3-pyridinium (**7**) and 4-phenyl substituted (**5**) dyes showed excellent (78.74% and 76.12%), and 3-amido substituted dye (**6**) expressed good

(62.22%) ability to scavenge the $ABTS^{\bullet+}$ radical cation, comparing to the inhibition of ascorbic acid (99.19%). Other investigated dyes exhibited moderate to weak antioxidant properties.

The promising candidates **5**, **6** and **7** have been further evaluated by determination of $IC_{50}$ values, which correspond to the concentration of sample able to scavenge 50% of ABTS radicals in the solution (Figure 6b). High $IC_{50}$ values generally suggest low antioxidant activity. The $IC_{50}$ values of samples, ranged from 1.26 to 1.63 mM, indicate that investigated dyes demonstrate good antioxidant capacity comparing to $IC_{50}$ value of ascorbic acid (1.09 mM). Based on the comparison of the $IC_{50}$ values, activity of the dyes was found to be as follows: 7 > 5 > 6.

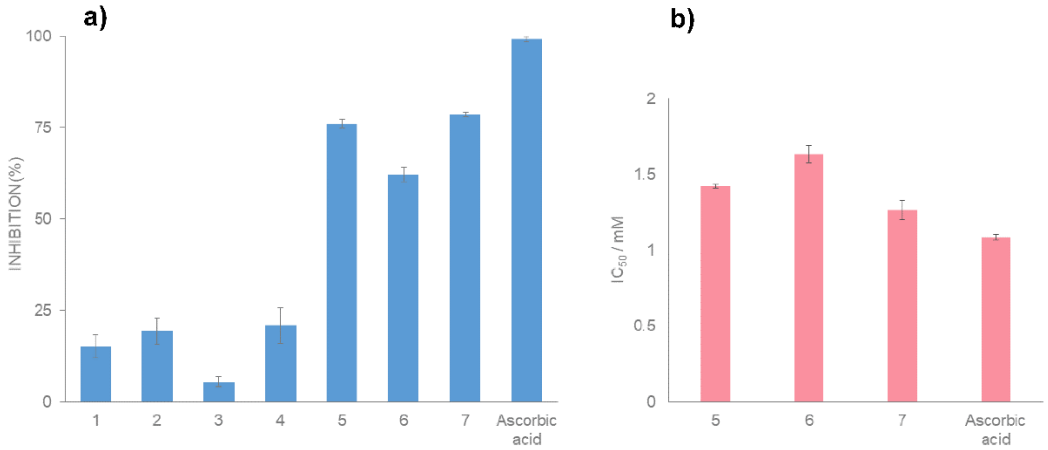


Figure 6. The antioxidant properties of investigated dyes compared to the ascorbic acid. a) The scavenging activity; b) The $IC_{50}$ values of dyes **5**, **6**, **7**.

*3.7. Cytotoxic activity*

The cytotoxic activity of **B2** and dyes **1–7** was examined against three human cancer cell lines, as well as on human normal lung fibroblasts using MTT assay (Table 4). Examination of the cytotoxic effects of the investigated compounds on human cancer cell lines showed concentration dependent cytotoxicity of all tested compounds (Table 4). Considering the cytotoxic activity of the compounds on human prostate adenocarcinoma PC-3 cells, the measured $IC_{50}$ values ranged from

48.98 µM do 194.41 µM. PC-3 cells were the most sensitive to the cytotoxicity of the compound **5** ($IC_{50}$ value of 48.98 µM). Tested compounds exerted cytotoxic effects on chronic myelogenous leukemia K562 cells, with $IC_{50}$ values of 24.97–193.32 µM. The highest intensity of the cytotoxic activity on K562 cells showed compounds **5** ($IC_{50}$ value of 24.97 µM), **3** ($IC_{50}$ value of 41.75 µM), and **6** ($IC_{50}$ value of 55.40 µM). The compounds exhibited weaker cytotoxic activity against human lung carcinoma A549 cells when compared with these activities against PC-3 and K562 cancer cells. The A549 cells were the most sensitive to the cytotoxicity of the compound **5** ($IC_{50}$ value of 85.16 µM). All examined compounds showed cytotoxicity against normal human lung fibroblasts MRC-5, with $IC_{50}$ values of 23.60–194.56 µM. It can be noted that assayed cancer cell lines were the most sensitive to the cytotoxic effect of the compound **5**. Furthermore, **5** was selective in cytotoxic action against PC-3 and K562 cells when compared with this activity against normal MRC-5 cells.

Besides, it can be seen from Table 4, that Biginelli adduct **B2** expressed very low cytotoxic activity against all investigated cancer cell lines, as well as against normal cells. This confirmed that cytotoxic activity of the investigated dyes depends on the structure of pyridone moiety. Furthermore, it can be noted that phenyl group on the pyridone moiety, at position C4 in the structure of dye **5**, was important for the cytotoxic activity against all tested cancer cell lines. However, the promising anticancer action gives compound **5** an attractive lead for further structural optimization.

Table 4. *In vitro* cytotoxic activities of the investigated compounds [$IC_{50}$[a] (µM) ± SD].

| | **PC-3** [b] | **A549** [b] | **K562** [b] | **MRC-5** [b] |
|---|---|---|---|---|
| **1** | 182.12±1.75 | >200 | 191.50±12.02 | 179.64±11.05 |
| **2** | 174.60±1.12 | >200 | 144.80±0.55 | ≈200 |
| **3** | 147.89±5.24 | >200 | 41.75±1.54 | 42.49±1.70 |
| **4** | 194.41±9.18 | >200 | 193.32±6.66 | 194.56±9.43 |
| **5** | 48.9848±1.59 | 85.16±6.03 | 24.97±0.05 | 91.11±5.33 |

| | | | | |
|---|---|---|---|---|
| **6** | 163.21±0.97 | 197.82±3.09 | 55.40±3.56 | 23.60±1.58 |
| **7** | 181.31±9.35 | 191.14±12.54 | 133.45±4.99 | 176.26±3.70 |
| **B2** | 169.53±5.34 | >200 | 149.10±9.53 | 153.66±7.26 |
| **CDDP**[c] | 12.29 ± 1.60 | 12.74 ± 1.26 | 5.90±0.59 | 5.74±0.48 |

[a]Cytotoxicity, $IC_{50}$ for each cell line, is the concentration of compound which reduced by 50% survival of treated cells with respect to untreated cells using the MTT assay. [b]Cell lines include human prostate adenocarcinoma (PC-3), lung carcinoma (A549), chronic myelogenous leukemia (K562) and human normal lung fibroblasts MRC-5. [c]Cisplatin – standard reference drug.

*3.8. Cell cycle analysis*

The cell cycle represents an ordered series of phases that occur during the cell division [49]. The main role of the cell cycle is to accomplish duplication and distribution of DNA content to newly divided daughter cells. The cell cycle is consistent of G1, S, G2 and M phases. DNA replication takes place in S phase, while in M phase replicated DNA is distributed to the new cells. Between M and S phase there is a phase called G1 (gap 1), and between S and M phase there is another phase called G2 phase (gap 2). The cells in G1 phase have normal DNA content, and cells in G2 phase have duplicated DNA content. All phases of the cell cycle undergo the checkpoint control, which provides the cell to ensure the cell cycle progression. However, cancer cells characterize the disrupted cell cycle progression, lack of the appropriate checkpoint control and the absence of cell death. Thus, the initiation of the cell death in cancer cells represents an effective anticancer therapy. The effect of compound **5** on the cell cycle distribution of K562 cells is studied, in order to investigate its possible mechanism of action (Figure 7). To determine whether the decrease in cell viability involved cell cycle distribution, cell cycle analysis was conducted by flow cytometry as previously described.

Treatment of human myelogenous leukemia K562 cells with $2IC_{50}$ concentration of the compound **5** for 24 h induced increase in the percentage of cells in the subG1 phase, which is followed by the increase in the percentage of cells in the G2/M phase, comparing to the control cell sample. The subG1 cell population represents dead cells with reduced DNA content. Therefore, the observed

increase of cells within subG1 cell cycle phase appoints the ability of compound **5** to induce cell death in treated K562 cells. The compound **5** also caused a cell cycle arrest of treated K562 cells within G2/M phase. The observed G2/M cell cycle arrest might be due to inhibition of cells to enter mitosis at G2/M checkpoint or to inhibition of cell progression through mitosis – M phase arrest. These changes in treated cells were accompanied with decrease in the percentage of cells within G1 and S phases. The reduced populations of treated K562 cells within G1 and S phases may suggest the increased sensitivity of cells within those cell cycle phases to the cytotoxic action of compound **5** [49, 50].

Taken together, the results of this research may suggest the possible anticancer potential of compound **5**, which may serve as a starting point for development of novel antitumor agents.

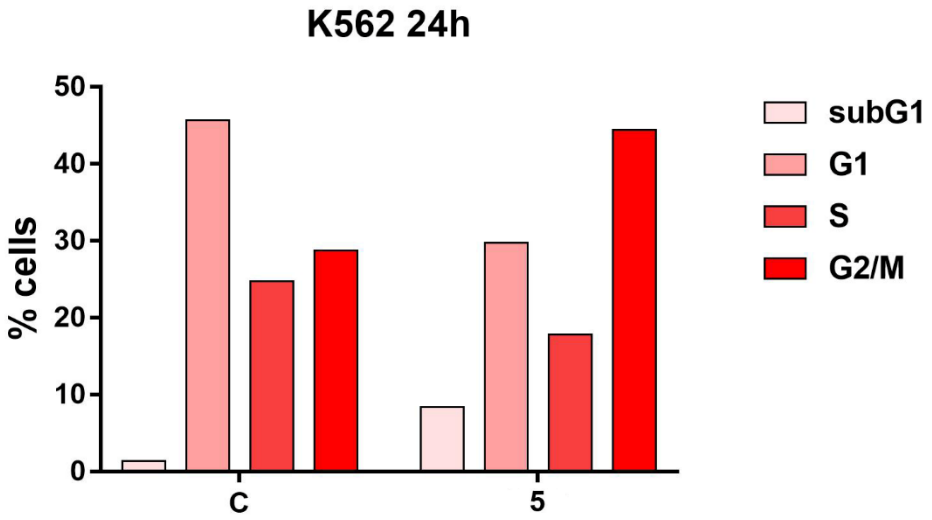


Figure 7. The changes in the cell cycle phase distribution of human chronic myelogenous leukemia K562 cells treated with $2IC_{50}$ concentration of the compound **5** after 24 h treatment.

*3.9. In silico assessment of physicochemical and ADME properties*

The investigated dyes **1**–**7** were profiled in the computational study of physicochemical and ADME (absorption, distribution, metabolism, and excretion) properties, using SwissADME [38,51]. The physicochemical parameters and drugability of the examined compounds were evaluated with respect to the Lipinski's rule of 5 (RO5) [52]. According to the Lipinski's rule, an orally active compound has to satisfy following criteria: i) the number of hydrogen bond donors is not greater than 5 (donors being N–H and O–H groups); ii) the number of hydrogen bond acceptors is maximum 10 (acceptors being N or O atoms); iii) a molecular weight is less than 500 and iv) lipophilicity (octanol/water partition coefficient – logP) is lower than 5. When a compound violates two or more of the stated rules it will likely have poor absorption or bioavailability. The physicochemical parameters for the hydrazone tauromeric (**1**–**7**) and zwitter ionic (**7a**) forms, calculated by SwissADME, are presented in Table 5.

Table 5. The physicochemical properties of investigated compounds.

| Dye | HBD[a] | HBA[b] | M log *P*[c] | MW[d] | Lipinski's violations[e] | %ABS[g] | Rot. Bond[g] |
|---|---|---|---|---|---|---|---|
| **1** | 4 | 7 | 0.37 | 436.42 | 1 | 53.19 | 6 |
| **2** | 4 | 8 | 0.05 | 480.47 | 1 | 49.24 | 8 |
| **3** | 3 | 7 | 1.01 | 478.50 | 1 | 56.22 | 8 |
| **4** | 3 | 7 | 1.68 | 512.52 | 2 | 56.22 | 7 |
| **5** | 4 | 7 | 1.21 | 498.49 | 1 | 53.19 | 7 |
| **6** | 5 | 7 | 0.02 | 454.44 | 1 | 46.53 | 7 |
| **7** | 4 | 6 | 1.08 | 489.50 | 1 | 60.05 | 7 |
| **7a** | 3 | 7 | 1.08 | 488.50 | 1 | 64.21 | 7 |

[a]The number of hydrogen bond donors; [b]The number of hydrogen bond acceptors; [c]The octanol/water partition coefficient, [d]The molecular weight; [e]The number of Lipinski's rule violation; [f]The number of rotatable bonds.

All investigated compounds, except compound **4**, can be considered as orally bioavailable, because they violate only one of the Lipinski's rule (N plus O atoms > 10, bioavailability score 0.55). The compound **4** has two violations of the stated rules (N plus O atoms > 10 and MW > 500,

bioavailability score 0.17) and thus, may be considered poorly orally active. It can be seen from the Table 5 that parameters obtained for the both structures, **7** and **7a,** fit the Lipinski's rule. Furthermore, absorption was calculated [53], and the obtained values were within the range of 46.53–64.21% which demonstrated that synthesized compounds have adequate cell membrane permeability and bioavailability. The number of rotatable bonds is another important parameter which is associated with good bioavailability. If the number of rotatable bonds is greater than 10, conformational flexibility of a molecule increases and binding to a biological target is difficult. The number of rotatable bonds of the investigated dyes is between 6 and 8, which indicates possibility for binding to active site [54].

The pharmacokinetics parameters, such as blood brain barrier permeability, the ability of a compound to be the P-gp (permeability glycoprotein) substrate and CYP (cytochrome enzymes) inhibitor, were analyzed (Table S2, Supplementary material). All investigated compounds have shown no permeation to the blood brain barrier, thus side effects to the central nervous system are prevented [53]. The P-gp is a key player in the process of an active efflux through biological membranes, and along with the CYPs it participates in the excretion processes [55]. All investigated structures were found to be the substrates of the P-gp, except the **7**. Furthermore, the pharmacokinetics parameters for CYPs inhibition have shown that novel dyes express no inhibition of CYPs, excluding dye **3** and **4** which inhibit CYP2C9 enzyme.

Finally, the medical chemistry results, such as PAINS (pan assay interference structures) alerts and synthetic accessibility scores, were analyzed (Table S2, Supplementary material). The PAINS are molecules containing the moieties that often give false positive biological output [56]. Among the structures under evaluation, only one structure, hydrazone tautomeric form of the **7**, displayed PAINS alert. Synthetic accessibility scores of novel dyes were found to be between 4.66 and 5.02

(in the scale where 1 is very easy and 10 is very difficult) indicating their relatively easy preparation.

In addition, some physicochemical descriptors such as lipophilicity (logP (Broto), lipole (Broto), virtual logP), polar and apolar surface area, gyration radius, volume and ovality of the investigated dyes, were estimated by Vega 22 (Table S3, Supplementary material). In contrast to SwissADME evaluation, wherein mentioned descriptors have been determined based on 2D structures of molecules, Vega 22 employed 3D structures of the optimized geometries, for the calculation of related parameters.

Since lipophilicity affects pharmacodynamics action of the compound, it has the significant impact on absorption, distribution, metabolism and excretion properties of the drug. The parameters regarding the lipophilicity (logP (Broto), lipole (Broto), virtual logP) are given in Table S3, Supplementary material. It can be concluded that all investigated compounds satisfy the principal drug-like property, the logP < 5, which is fundamental for the success in drug development [57].

## 4. Conclusion

In this work seven novel azo pyridone dyes based on dihydropyrimidinone scaffold have been synthesized, and their structures have been confirmed experimentally and theoretically. ATR-FTIR and NMR spectroscopy confirmed that obtained dyes **1**–**6** exist in hydrazone tautomeric form, whereas dye **7** exist in zwitter ionic form, in solid state, as well as in DMSO-$d_6$ solution. The conformational analysis was conducted and the optimized geometries of the most stable conformers of dye **1** were obtained with B3LYP method. The largest conformational difference in the molecule resulted from the rotation of the DHPM group around the C14–C20 bond. The vibrational and NMR spectral analysis have shown that experimental spectra correlate well with the calculated data, which was powerful confirmation of the hydrazone structure. Furthermore,

MEP maps revealed that the sites for the electrophilic attacks are around the carbonyl oxygen atoms and nitrile group of pyridone ring, while possible sites for nucleophilic attacks are around hydrogen atoms belonging to two N-H groups of DHPM. According to the calculated QCDs, the molecules **7a** and **5** showed prominent reactivity. The highest antioxidant activity whit respect to $IC_{50}$ value manifested dyes **5** (1.42 mM), **6** (1.63 mM) and **7** (1.26 mM), comparing to the $IC_{50}$ value of ascorbic acid (1.09 mM). Evaluation of *in vitro* cytotoxic activity of investigated compounds, on human cancer cell lines PC-3, K562 and A549, showed the concentration dependent cytotoxicity. The cytotoxic activity of the investigated dyes depends on the structure of pyridone moiety since the Biginelli adduct **B2** expressed low cytotoxic activity against all investigated cancer cell lines. All tested cancer cell lines were the most sensitive to the cytotoxic action of **5**, while noticeable selectivity in cytotoxic activity is observed between human cancer cell lines (PC-3 and K562) and normal (MRC-5) cells. Moreover, the cell cycle analysis of **5**, examined in K562 cells, show the increase in percentage of cells within subG1 phase, which indicates cell death. Also, **5** induces the cycle arrest within G2/M phase, affecting the decrease in the percentage of cells within G1 and S phases, which suggests the increased sensitivity of cells to the cytotoxic action of compound **5**. The ADME evaluation *in silico* has shown that all investigated compounds may be orally bioavailable with no permeation to the blood brain barrier. In addition, lipophilicity parameters indicate that all compounds satisfy the principal drug-like property, the log $P < 5$, which is fundamental for the success in drug development. Altogether, it can be concluded that novel dyes may serve for further structural modification and development of new anticancer drugs.

**Acknowledgement**

This work was supported by the Ministry of Education, Science and Technological Development of the Republic of Serbia (Contract No. 451-03-68/2020-14/200287, 451-03-68/2020-14/200026, 451-03-68/2020-14/200135 and 451-03-68/2020-14/200043).

## References

[1] Zollinger H. Color chemistry: synthesis, properties and application of organic dyes and pigments. Weinheim: Wiley-VCH; 2003.

[2] Metwally MA, Abdel-Galil E, Metwally A, Amer FA. New azodisperse dyes with thiazole, thiophene, pyridone and pyrazolone moiety for dyeing polyester fabrics. Dyes Pigments 2012;92:902–8. https://doi.org/https://doi.org/10.1016/j.dyepig.2011.07.009.

[3] Tao T, Zhao X, Wang Y, Qian H, Huang W. 5-Hydroxy-1-phenyl-1H-pyrazole-3-carboxylic acid based heterocyclic dyes. Dyes Pigments 2019;166:226–32. https://doi.org/https://doi.org/10.1016/j.dyepig.2019.03.046.

[4] Mishra VR, Ghanavatkar CW, Sekar N. UV protective heterocyclic disperse azo dyes: Spectral properties, dyeing, potent antibacterial activity on dyed fabric and comparative computational study. Spectrochim Acta A 2019;223:117353. https://doi.org/https://doi.org/10.1016/j.saa.2019.117353.

[5] Ali HM, Badr SQ, Temma AS. Synthesis and biological studies of some diazo dyes as new drugs. Int J Drug Deliv Technol 2019;9:613–6. https://doi.org/10.25258/ijddt.v9i4.16.

[6] Ghasemian M, Kakanejadifard A, Azarbani F, Zabardasti A, Kakanejadifard S. Spectroscopy and solvatochromism studies along with antioxidant and antibacterial activities investigation of azo–azomethine compounds 2-(2-hydroxyphenylimino)methyl)-4-phenyldiazenyl)phenol. Spectrochim Acta A 2014;124:153–8. https://doi.org/https://doi.org/10.1016/j.saa.2014.01.005.

[7] Smith HS, Lesar TS. Analgesic prescribing errors and associated medication characteristics. J Pain 2011;12:29–40. https://doi.org/10.1016/j.jpain.2010.04.007.

[8] Li X, Li J, Gao Y, Kuang Y, Shi J, Xu B. Molecular Nanofibers of Olsalazine Form Supramolecular Hydrogels for Reductive Release of an Anti-inflammatory Agent. J Am Chem Soc 2010;132:17707–9. https://doi.org/10.1021/ja109269v.

[9] Wainwright M. Dyes in the development of drugs and pharmaceuticals. Dyes Pigments 2008;76:582–9. https://doi.org/https://doi.org/10.1016/j.dyepig.2007.01.015.

[10] Afifi TH, Riyadh SM, Deawaly AA, Naqvi A. Novel chromenes and benzochromenes bearing arylazo moiety: molecular docking, in-silico admet, in-vitro antimicrobial and anticancer screening. Med Chem Res 2019;28:1471–87. https://doi.org/10.1007/s00044-019-02387-5.

[11] Ghasemi Z, Azizi S, Salehi R, Kafil HS. Synthesis of azo dyes possessing *N*-heterocycles and evaluation of their anticancer and antibacterial properties. Monatsh Chem 2018;149:149–57. https://doi.org/10.1007/s00706-017-2073-y.

[12] Sahoo J, Paidesetty SK. Medicinal interest of AZO-based organic compounds: A review. Asian J Pharm Clin Res 2016;9:33–9.

[13] Ashkar SM, El-Apasery MA, Touma MM, Elnagdi MH. Synthesis of some novel biologically active disperse dyes derived from 4-methyl-2,6-dioxo-1-propyl-1,2,5,6-tetrahydropyridine-3-carbonitrile as coupling component and their colour assessment on polyester fabrics. Molecules 2012;17:8822–31. https://doi.org/10.3390/molecules17088822.

[14] Karcı F, Karcı F, Demirçalı A, Yamaç M. Synthesis, solvatochromic properties and antimicrobial activities of some novel pyridone-based disperse disazo dyes. J Mol Liq 2013;187:302–8. https://doi.org/https://doi.org/10.1016/j.molliq.2013.08.005.

[15] Mijin D, Božić Nedeljković BB, Božić B, Kovrlija I, Ladarević J, Uščumlić G. Synthesis, solvatochromism, and biological activity of novel azo dyes bearing 2-pyridone and benzimidazole moieties. Turk J Chem 2018;42:896–907. https://doi.org/10.3906/kim-1711-97.

[16] Peng Q, Li M, Gao K, Cheng L. Hydrazone-azo tautomerism of pyridone azo dyes: Part 1—NMR Spectra of Tautomers. Dyes Pigments 1990;14:89–99. https://doi.org/https://doi.org/10.1016/0143-7208(90)87009-R.

[17] Peng Q, Li M, Gao K, Cheng L. Hydrazone-azo tautomerism of pyridone azo dyes: Part II: Relationship between structure and pH values. Dyes Pigments 1991;15:263–74. https://doi.org/https://doi.org/10.1016/0143-7208(91)80011-W.

[18] Peng Q, Li M, Gao K, Cheng L. Hydrazone-azo tautomerism of pyridone azo dyes: Part III—effect of dye structure and solvents on the dissociation of pyridone azo dyes. Dyes Pigments 1992;18:271–86. https://doi.org/https://doi.org/10.1016/0143-7208(92)80017-H.

[19] Katritzky AR, Hall CD, El-Gendy BEM, Draghici B. Tautomerism in drug discovery. J Comput Aid Mol Des 2010;24:475–84. https://doi.org/10.1007/s10822-010-9359-z.

[20] Kappe CO. Recent Advances in the Biginelli Dihydropyrimidine Synthesis. New Tricks from an Old Dog. Accounts Chem Res 2000;33:879–88. https://doi.org/10.1021/ar000048h.

[21] Stadler A, Kappe CO. Automated Library Generation Using Sequential Microwave-Assisted Chemistry. Application toward the Biginelli Multicomponent Condensation. J Comb Chem 2001;3:624–30. https://doi.org/10.1021/cc010044j.

[22] de Fátima Â, Braga TC, Neto L da S, Terra BS, Oliveira BGF, da Silva DL, et al. A mini-review on Biginelli adducts with notable pharmacological properties. J Adv Res 2015;6:363–73. https://doi.org/https://doi.org/10.1016/j.jare.2014.10.006.

[23] Liu Y, Liu J, Zhang R, Guo Y, Wang H, Meng Q, et al. Synthesis, characterization, and anticancer activities evaluation of compounds derived from 3,4-dihydropyrimidin-2(1*H*)-one. Molecules 2019;24:891–909. https://doi.org/10.3390/molecules24050891.

[24] Zabihollahi R, Fassihi A, Aghasadeghi MR, Memarian HR, Soleimani M, Majidzadeh-A K. Inhibitory effect and structure–activity relationship of some Biginelli-type pyrimidines against HSV-1. Med Chem Res 2013;22:1270–6. https://doi.org/10.1007/s00044-012-0123-x.

[25] Shaikh A, Meshram JS. Design, synthesis and pharmacological assay of novel azo derivatives of dihydropyrimidinones. Cogent Chem 2015;1:1019809. https://doi.org/10.1080/23312009.2015.1019809.

[26] Mathapati SR, Swami MB, Jadhav AH, Ghule NV, Dawle JK. Design and synthesis of classical dihydropyrimidone derivatives from azosalicyaldehydes. Der Pharma Chem 2017;9:1–5.

[27] Matović L, Tasić N, Trišović N, Lađarević J, Vitnik V, Vitnik Ž, et al. On the azo dyes derived from benzoic and cinnamic acids used as photosensitizers in dye-sensitized solar cells. Turkish J Chem 2019;43:1183–203. https://doi.org/10.3906/kim-1903-76.

[28] Tadić J, Mihajlović M, Jovanović M, Mijin D. Continuous flow synthesis of some 6- and 1,6-substituted 3-cyano-4-methyl-2-pyridones. J Serb Chem Soc 2019;84:531–8. https://doi.org/10.2298/JSC180703092T.

[29] Jiyunji T, Hiroyuki M. Preparation of 6-hydroxypyrid-2-ones. 1981. JP 56012369.

[30] Frisch MJ, Trucks GW, Schlegel HB, Scuseria GE, Robb MA, Cheeseman JR, et al. Gaussian 09, Revision D.01. Wallingford CT: Gaussian, Inc.; 2009.

[31] Andersson MP, Uvdal P. New Scale Factors for Harmonic Vibrational Frequencies Using the B3LYP Density Functional Method with the Triple-ζ Basis Set 6-311+G(d,p). J Phys Chem A 2005;109:2937–41. https://doi.org/10.1021/jp045733a.

[32] Dennington R, Keith T, Millam J. GaussView, Version 5.0.9. Shawnee Mission, KS: Semichem Inc.; 2009.

[33] Sayin K, Üngördü A. Investigations of structural, spectral and electronic properties of enrofloxacin and boron complexes via quantum chemical calculation and molecular docking. Spectrochim Acta A 2019;220:117102. https://doi.org/10.1016/j.saa.2019.05.007.

[34] Re R, Pellegrini N, Proteggente A, Pannala A, Yang M, Rice-Evans C. Antioxidant activity applying an improved ABTS radical cation decolorization assay. Free Radical Biol Med 1999;26:1231–7. https://doi.org/10.1016/S0891-5849(98)00315-3.

[35] Mosmann T. Rapid colorimetric assay for cellular growth and survival: application to proliferation and cytotoxicity assays. J Immunol Methods. 1983;65(1–2):55–63. https://doi.org/10.1016/0022-1759(86)90368-6.

804 [36] Ohno M, Abe T. Rapid colorimetric assay for the quantification of leukemia inhibitory factor (LIF)
805 and interleukin-6 (IL-6). J Immunol Methods. 1991;145(1–2):199–203. https://doi.org/10.1016/0022-
806 1759(91)90327-C.
807 [37] Ormerod MG. Flow cytometry. A practical approach. Oxford University Press 2000.
808 [38] A free web tool to evaluate pharmacokinetics, drug-likeness and medicinal chemistry friendliness,
809 www.swissadme.ch; Swiss Institute of Bioinformatics 2019 [accessed October 2020].
810 [39] Pedretti A, Villa L, Vistoli G. VEGA – An open platform to develop chemo-bio-informatics
811 applications, using plug-in architecture and script programming. J Comput Aid Mol Des 2004;18:167–
812 73. https://doi.org/10.1023/B:JCAM.0000035186.90683.f2.
813 [40] Mirković J, Rogan J, Poleti D, Vitnik V, Vitnik Ž, Uščumlić G, et al. On the structures of 5-(4-, 3- and
814 2-methoxyphenylazo)-3-cyano-1-ethyl-6-hydroxy-4-methyl-2-pyridone: An experimental and
815 theoretical study. Dyes Pigments 2014;104:160–8.
816 https://doi.org/https://doi.org/10.1016/j.dyepig.2014.01.007.
817 [41] Mirković J, Božić B, Vitnik V, Vitnik Ž, Rogan J, Poleti D, et al. Structural, spectroscopic and
818 computational study of 5-(substituted phenylazo)-3-cyano-1-ethyl-6-hydroxy-4-methyl-2-pyridones.
819 Color Technol 2017;134:33–43. https://doi.org/10.1111/cote.12321.
820 [42] Mirković JM, Božić BĐ, Mutavdžić DR, Uščumlić GS, Mijin DŽ. Solvent and structural effects on
821 the spectral shifts of 5-(substituted phenylazo)-3-cyano-6-hydroxy-1-(2-hydroxyethyl)-4-methyl-2-
822 pyridones. Chem Phys Lett 2014;615:62–8.
823 https://doi.org/https://doi.org/10.1016/j.cplett.2014.09.063.
824 [43] Lađarević J, Božić B, Matović L, Nedeljković BB, Mijin D. Role of the bifurcated intramolecular
825 hydrogen bond on the physico-chemical profile of the novel azo pyridone dyes. Dyes Pigments
826 2019;162:562–72. https://doi.org/https://doi.org/10.1016/j.dyepig.2018.10.058.
827 [44] Porobić SJ, Božić BĐ, Dramićanin MD, Vitnik V, Vitnik Ž, Marinović-Cincović M, et al. Absorption
828 and fluorescence spectral properties of azo dyes based on 3-amido-6-hydroxy-4-methyl-2-pyridone:

Solvent and substituent effects. Dyes Pigments 2020;175:108139. https://doi.org/https://doi.org/10.1016/j.dyepig.2019.108139.

[45] Mijin D, Božić B, Lađarević J, Matović L, Uščumlić G, Vitnik V, et al. Solvatochromism and quantum mechanical investigation of disazo pyridone dye. Color Technol 2018;134:478–90. https://doi.org/10.1111/cote.12369.

[46] Sayin K, Kariper SE, Taştan M, Sayin TA, Karakaş D. Investigations of structural, spectral, electronic and biological properties of *N*-heterocyclic carbene Ag(I) and Pd(II) complexes. J Mol Struct 2019; 1176:478-487. https://doi.org/10.1016/j.molstruc.2018.08.103.

[47] Erkan S. Activity of the rocuronium molecule and its derivatives: A theoretical calculation. J Mol Struct 2019;1189:257–64. https://doi.org/10.1016/j.molstruc.2019.04.042.

[48] Kökbudak Z, Saracoglu M, Akkoç S, Çimen Z, Yilmazer MI, Kandemirli F. Synthesis, cytotoxic activity and quantum chemical calculations of new 7-thioxopyrazolo[1,5-f]pyrimidin-2-one derivatives. J Mol Struct 2020;1202:127261. https://doi.org/10.1016/j.molstruc.2019.127261.

[49] Mukherjee S, Mitra I, Reddy V, Fouzder C, Mukherjee S, Ghosh S, et al. Effect of Pt(II) complexes on cancer and normal cells compared to clinically used anticancer drugs: cell cycle analysis, apoptosis and DNA/BSA binding study. J Mol Liq 2017;247:126–40. https://doi.org/10.1016/j.molliq.2017.09.104.

[50] Keleş T, Barut B, Özel A, Biyiklioglu Z. Synthesis of water soluble silicon phthacyanine, naphthalocyanine bearing pyridine groups and investigation of their DNA interaction, topoisomerase inhibition, cytotoxic effects and cell cycle arrest properties. Dyes Pigments 2019;164:372–83. https://doi.org/10.1016/j.dyepig.2019.01.044.

[51] Daina A, Michielin O, Zoete V. SwissADME: a free web tool to evaluate pharmacokinetics, drug-likeness and medicinal chemistry friendliness of small molecules. Sci Rep 2017;7:42717. https://doi.org/10.1038/srep42717.

[52] Lipinski CA, Lombardo F, Dominy BW, Feeney PJ. Experimental and computational approaches to estimate solubility and permeability in drug discovery and development settings. Adv Drug Deliver Rev 1997;23:3–25. https://doi.org/https://doi.org/10.1016/S0169-409X(96)00423-1.

[53] Ismail MMF, Farrag AM, Harras MF, Ibrahim MH, Mehany ABM. Apoptosis: A target for anticancer therapy with novel cyanopyridines. Bioorg Chem 2020;94:103481. https://doi.org/10.1016/j.bioorg.2019.103481.

[54] Veber DF, Johnson SR, Cheng HY, Smith BR, Ward KW, Kopple KD. Molecular Properties That Influence the Oral Bioavailability of Drug Candidates. J Med Chem 2002;45:2615–23. https://doi.org/10.1021/jm020017n.

[55] Kim RB, Wandel C, Leake B, Cvetkovic M, Fromm MF, Dempsey PJ, et al. Interrelationship between substrates and inhibitors of human CYP3A and P-glycoprotein. Pharm Res. 1999;16:408–14. doi: 10.1023/a:1018877803319.

[56] Jonathan BB, Georgina AH. New Substructure Filters for Removal of Pan Assay Interference Compounds (PAINS) from Screening Libraries and for Their Exclusion in Bioassays. J Med Chem 2010;53:2719–40. doi: 10.1021/jm901137j.

[57] Leeson PD, Springthorpe B. The influence of drug-like concepts on decision-making in medicinal chemistry. Nat Rev Drug Discov 2007;6:881–90. doi: 10.1038/nrd2445.